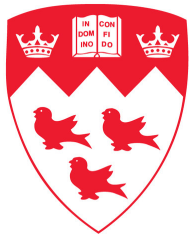


Brillouin Thulium Doped Fiber Laser at $1.9 \mu\text{m}$ and Bismuth Doped Fiber Laser at $1.7 \mu\text{m}$

Jinghao Qiao



McGill

Photonics System Group

Department of Electrical and Computer Engineering

McGill University

Montreal, Quebec, Canada

July 2018

A thesis submitted to McGill University in partial fulfillment of the
requirements of the degree of Master of Engineering

©Jinghao Qiao, 2018

Abstract

The high and rapidly increasing demand for more telecommunication capacity and internet services drives the evolution of fiber optic communication. The third telecom window, which utilizes wavelengths around $1.5\ \mu\text{m}$ and is widely utilized nowadays, can not meet this demand in future. Researchers are trying to develop technologies in new wavelength regions. Longer wavelength region has attracted intense interests for its prospective application. On the other hand, the fact that the wavelength region from $1.7\ \mu\text{m}$ to $2\ \mu\text{m}$ covers the absorption bands of water and greenhouse gas facilitates the applications in such area as sensing, spectroscopy and coherent LIDAR. In this thesis, we demonstrate a multi-wavelength thulium doped fiber laser around $1.9\ \mu\text{m}$ and a bismuth doped fiber laser around $1.7\ \mu\text{m}$.

The $1.9\ \mu\text{m}$ multi-wavelength laser uses a combination of a 25 cm Tm^{3+} -doped silica fiber along with stimulated Brillouin scattering and four wave mixing. More than 100 lines can be observed in the optical spectrum. It is, to the best of our knowledge, the largest number of lasing wavelengths emitting from a Brillouin thulium fiber laser. The peak wavelengths drift less than 0.02 nm and peak powers fluctuate less than 3.4 dB in 20 minutes.

The $1.7\ \mu\text{m}$ CW laser uses a 15 m bismuth doped germanosilicate fiber as active fiber. Both linear cavity and ring cavity are tried to build laser. With linear cavity, a laser at 1726 nm has been achieved. The laser has maximum output power of $55\ \mu\text{W}$ with slope efficiency of 5.76×10^{-5} W/W. With ring cavity, the laser has maximum output power of $300\ \mu\text{W}$ with slope efficiency of 3.55×10^{-4} W/W. The laser has single-wavelength operation at 1735 nm or dual-wavelength operation at 1726 nm and 1735 nm.

Résumé

La forte et croissance rapide de la demande pour plus de capacité de télécommunications et de services internet stimule l'évolution des communications par fibres optiques. La troisième fenêtre de télécommunications, qui utilise des longueurs d'ondes autour de $1,5 \mu\text{m}$ et est largement utilisée de nos jours, ne pourra pas répondre à cette demande à l'avenir. Les chercheurs tentent de développer des technologies dans de nouvelles régions de longueur d'onde. Une région de plus grandes longueurs d'onde a suscité un vif intérêt pour ses applications potentielles. D'autre part, le fait que la zone de longueurs d'onde de $1,7 \mu\text{m}$ à $2 \mu\text{m}$ couvre les bandes d'absorption de l'eau et des gaz à effet de serre facilite les applications dans des domaines tels que la détection, la spectroscopie et le LIDAR cohérent. Dans cette thèse, nous démontrons un laser à fibre dopée au thulium à longueurs d'onde multiples autour de $1,9 \mu\text{m}$ et un laser à fibre dopée au bismuth autour de $1,7 \mu\text{m}$.

Le laser à longueurs d'onde multiples autour de $1,9 \mu\text{m}$ utilise une fibre de silice dopée au Tm^{3+} de 25 cm en combinaison avec la diffusion de Brillouin stimulée et le mélange à quatre ondes. Plus de 100 lignes peuvent être observées dans le spectre optique. Il s'agit, à notre connaissance, du plus grand nombre de longueurs d'onde laser émises par un laser à fibre dopée au thulium de type Brillouin. Les longueurs d'onde crêtes dérivent de moins de 0,02 nm et les puissances crêtes fluctuent de moins de 3,4 dB en 20 minutes.

Le laser CW autour de $1,7 \mu\text{m}$ utilise une fibre de silicate de germanium dopée au bismuth de 15 m comme fibre active. Une cavité linéaire et une cavité annulaire sont testées pour construire le laser. Avec une cavité linéaire, un laser émettant à 1726 nm a été réalisé. Le laser a une puissance de sortie maximale de $55 \mu\text{W}$ avec une efficacité de pente de $5,76 \cdot 10^{-5}$ W/W. Avec la cavité annulaire, le laser a une puissance de sortie maximale de $300 \mu\text{W}$ avec une efficacité de pente de $3,55 \cdot 10^{-4}$ W/W. Le laser opère à une longueur d'onde unique de 1735 nm ou aux deux longueurs d'onde de 1726 nm et 1735 nm.

Acknowledgement

First of all, I would like to express sincere gratitude to my supervisor Prof. Lawrence Chen. He has always been helpful and supportive to his students. I appreciate him for spending time viewing my reports and giving me feedback. He can always provide valuable advices to solve my experimental problems. His enthusiasm and profound erudition always encourage me. It is my honor to be his student.

I would like to thank the other professors in photonic system group. Their contribution and management make our group a world-class photonic research group. Special thanks to Prof. Martin Rochette, who provided me with some experimental devices. I would like to thank Dr. Sergei Firstov at fiber optics research center in Moscow who provided me with bismuth doped fiber and helped me for experiments.

I would like to thank my friends and colleagues in photonic system group who helped me during my study: Dr. Chenglai Jia, Ms. Zifei Wang, Dr. Galina Nemova, Mr. Maxime Jacques, Mr. Bruno Taglietti, Dr. Jingjing Hu, Ms. Maria-Iulia Comanici, Dr. Reza Maram, Mr. Nurmemet Abdukerim Mr. Imtiaz Gabriel, Mr. Weixuan Lin and Mr. Huai Yang.

Last but not least, I appreciate my beloved parents for providing me with selfless love and continuous encouragement. This accomplishment would not have been possible without their support.

Contents

List of Figures	6
List of Abbriviations	9
1 Introduction	11
1.1 Introduction	11
1.2 Motivation and Objectives	12
1.3 Thesis Contribution	14
1.4 Thesis Outline	15
2 Background	16
2.1 Ion-doped Fibers	16
2.1.1 Tm ³⁺ doped fiber	16
2.1.2 Bismuth doped fiber	17
2.2 Fiber Optic Nonlinearities	19
2.2.1 Stimulated Brillouin Scattering	20
2.2.2 Four Wave Mixing	22
2.3 Review of Previous work	24
2.3.1 Review of Brillouin Fiber Lasers	24
2.3.2 Review of Bismuth Doped fiber laser	29
2.4 Summary	34
3 Multi-Wavelength Brillouin Tm³⁺-Doped Fiber Laser at 1874nm	35
3.1 Introduction	35

3.2	Tm ³⁺ Doped Fiber	36
3.3	Experimental Setup and Results	38
3.3.1	Brillouin Pump Laser	38
3.3.2	Home-Built Thulium Doped Fiber Amplifier	41
3.3.3	Linear Cavity of the Brillouin TDFL	44
3.3.4	Results and Discussion	45
3.4	Conclusion	50
4	CW Bismuth-Doped Fiber Lasers at 1726 nm	51
4.1	Introduction	51
4.2	Bismuth Doped Fiber	51
4.3	Experimental Setups and Results	56
4.3.1	BDFL with Linear Cavity	56
4.3.2	BDFL with Ring Cavity	58
4.4	Conclusion	60
5	Conclusion	61
5.1	Summary	61
5.2	Future work	61
	References	63

List of Figures

1.1	Spectral attenuation of a silica optical fiber (SMF-28)	12
2.1	Energy-level diagram of the Tm ³⁺ ion [19]	17
2.2	Energy-level diagram of (a) Si-BAC and (b) Ge-BAC [20]. ©2014, IEEE	18
2.3	Generation of new signals with ν_3 and ν_4 via FWM	23
2.4	Experimental laser configurations for (a) the first Brillouin EDFL and (b) the first multiple wavelength Brillouin EDFL.	24
2.5	Schematic diagram of the EDFA-enhanced Brillouin EDFL	25
2.6	Schematic diagram of BEFL with internal feedback	25
2.7	Configuration of the first Brillouin EDFL with a linear cavity	26
2.8	Setup of the multiwavelength Brillouin TDFL	27
2.9	Experimental configuration of the high signal to noise ratio, signal-frequency 2 μm Brillouin fiber laser	28
2.10	Experimental setup of the Hybrid Brillouin-thulium single-frequency fiber laser	28
2.11	Experimental setup of the first BDFL with linear cavity	29
2.12	Experimental setup of the first BDFL with ring cavity	30
2.13	Experimental setup of the CW high power BDFL	31
2.14	Mode-locked Bi-doped fiber laser configuration	31
2.15	High power BDFL configuration at 1.7 μm	32
2.16	The schematic of the mode-locked bismuth fiber laser operating in the anomalous dispersion regime	33
2.17	Schematic of the NALM-based BDFL at 1.7 μm	33

3.1	Experimental setup to measure Tm^{3+} :silica fiber ASE with (a) forward pump and (b) backward pump	36
3.2	Measured ASE spectra of 25 cm Tm^{3+} -doped silica fiber with forward pump and backward pump	37
3.3	Measured ASE spectra with different lengths of Tm^{3+} -doped fiber under a 2 W forward pump power	38
3.4	Setup of Brillouin pump laser with compound rings and saturable absorber .	39
3.5	The measured RF spectra of the Brillouin pump laser	40
3.6	(a) The optical spectrum of the Brillouin pump laser. (b) The output power of 1873.9 nm versus pump power at 1560 nm	40
3.7	(a) optical spectra measured in 20 minutes, (b) output power fluctuation in 20 minutes	41
3.8	Setup of thulium doped fiber amplifier	42
3.9	Experimental setup to measure the gain of the home-built TDFA	42
3.10	Optical spectra of the original backward ASE and amplified ASE	43
3.11	Gain at 1874 nm versus pump power for the Tm^{3+} doped fiber	43
3.12	Multi-wavelength Brillouin TDFL configuration	44
3.13	optical spectrum of the Brillouin TDFL when Brillouin pump power=70 mW, and TDFA2 pump power=1.5 W	46
3.14	Spectra of the Brillouin TDFL with the BP power fixed at 150 mW	46
3.15	Spectra of the Brillouin TDFL with the TDFA2 pump power fixed at 1.5 W	47
3.16	Experimental setup of the linear cavity laser	47
3.17	The optical spectra of the Brillouin TDFL and the linear cavity laser when the pump power is 1.5 W	48
3.18	Output spectra of Brillouin TDFL measured in 20 minutes	49
3.19	(a) wavelength fluctuations and (b) power fluctuations of four selected lasing peaks	49
4.1	Spectra variation of the emission and absorption cross section	52
4.2	Optical spectra of the ASE for the bismuth doped fiber	52

4.3	Experimental configurations to measure the gain of bismuth doped fiber with (a) forward pumping scheme and (b) backward pumping scheme	53
4.4	Optical spectra of the forward pumping scheme	54
4.5	Optical spectra of the backward pumping scheme	54
4.6	Gain spectra of bismuth doped fiber with forward pumping scheme	55
4.7	Gain spectra of bismuth doped fiber with backward pumping scheme	55
4.8	Gain at 1726 nm versus pump power for the bismuth doped fiber	56
4.9	Linear cavity BDFLs	57
4.10	Output spectra of linear cavity BDFLs	57
4.11	Output power with respect to the pump power for linear cavity BDFL	58
4.12	experimental setup of BDFL with ring cavity	59
4.13	Output power with respect to the pump power for ring cavity BDFL	59
4.14	Optical spectra of ring cavity BDFL	60

List of Abbreviations

ASE	Amplified spontaneous emission
BAC	Bismuth Active Center
BDFL	Bismuth doped fiber laser
BP	Brillouin pump
CNT	Carbon nanotube
CW	Continuous wave
DC	Double cladding
DWDM	Dense wavelength division multiplexing
ECL	External cavity laser
EDFA	Erbium doped fiber amplifier
EDFL	Erbium doped fiber laser
FBG	Fiber Bragg grating
FWHM	Full width at half maximum
FWM	Four wave mixing
HNLF	Highly nonlinear fiber
MCVD	Modified Chemical Vapour Deposition
MOPA	Monolithic master oscillator amplifier

NA	Numerical Aperture
NALM	Nonlinear amplifying loop mirror
OSA	Optical spectrum analyzer
OSNR	Optical signal to noise ratio
PC	Polarization controller
PDI	Polarization dependent isolator
RF	Radio frequency
SA	Saturable absorber
SBS	Stimulated Brillouin scattering
SLM	Single longitudinal mode
SMF	Single mode fiber
TDFA	Thulium doped fiber amplifier
TDFL	Thulium doped fiber laser
WDM	Wavelength division multiplexing

Chapter 1

Introduction

1.1 Introduction

The term “laser” is an acronym for “light amplification by stimulated emission of radiation”. In 1960, Theodore H. Mainman at Hughes Research Laboratories built the first laser with ruby [1]. The monochromaticity, coherence, high power density and tunability of laser make it an ideal light source for many important applications, such as optical communication, sensing, laser surgery, laser cutting and laser printer, etc. Researchers have made many different lasers for different applications.

These lasers share some common features, such as a pumping source to generate population inversion, an active medium to provide gain, an optical cavity to provide feedback [2]. However, the details of these features play an important role in differentiating the laser performance. Unlike the other traditional lasers using crystal rod or gas-filled tube as gain medium, fiber lasers, as their name suggest, usually utilize ion doped fibers as gain medium. This feature gives fiber lasers many advantages. Due to the large surface to volume ratio of fiber, fiber lasers have better performance in thermal management. Fiber lasers can have a very long active region, which supports a very high output power. Since fiber can be bent and coiled, fiber laser can be compact compared to rod or gas lasers of comparable power, and the fact that the light is already in a fiber make it convenient for fiber optic communication. These advantages make fiber lasers attract intense interests. They have achieved

great development last three decades since David Payne demonstrated erbium doped fiber amplifiers in 1987 for the first time [3].

1.2 Motivation and Objectives

From 1990, the optical communication in the 1550 nm transmission window has been developed greatly. It was determined by the attenuation characteristics of the silica glass used in fibers. At around 1550 nm, both Rayleigh scattering, OH^- absorption and infrared absorption are at a minimum, which make 1550 nm window suitable for fiber communication. For silica fiber, the lowest attenuation of about 0.18 dB/km can be achieved in 1550 nm, see Fig. 1.1. However, requests for higher transmission speed and larger transmission capacity make the only 1550 nm window cannot satisfy people's need in future. Researchers are looking for the next optical window and extending present laser sources to a wide variety of lasing wavelengths [4].

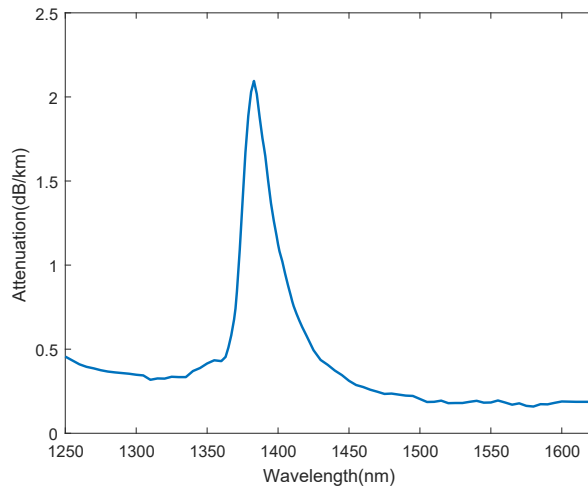


Figure 1.1: Spectral attenuation of a silica optical fiber (SMF-28)

Recently, the laser around $2 \mu\text{m}$ has attracted much attention and made rapid development. The wavelength is within the absorption bands of liquid water and greenhouse gases and the atmospheric transparency window, which facilitates the applications in the area of high-resolution spectroscopy, coherent LIDAR and free-space optical communications. Moreover, hollow core photonic bandgap fibers are recognized to be novel transmission medium

due to the ultra-low nonlinearity and faster transmission speed compared to traditional solid fibers [5], and they are predicted to have minimum attenuation at around 2 μm by both theoretical models and experimental results. That means optical communication at around 2 μm has the potential to overcome the capacity limit at 1550nm. Therefore, the laser sources at around 2 μm are important and need to be investigated further.

Thulium (Tm^{3+}) doped fiber amplifier (TDFA) offers a broad emission band from 1750 nm to 2050 nm, which coincides with the 2 μm operation window. Besides, the Tm^{3+} doped fiber laser (TDFL) has the advantage of high output power, high slope efficiency and eye safety. Therefore, the TDFL has attracted intensive interests. A widely-tunable and switchable dual-wavelength TDFL from 1857 nm to 1927 nm has been demonstrated [6]. A high power up to 115W all fiber wavelength-tunable from 1940 nm to 2070 nm TDFL based on a monolithic master oscillator power amplifier (MOPA) system with the slope efficiency of 51.7% has been presented [7]. A thulium doped passive mode-locked fiber laser at 1870 nm has been realized by using nonlinear amplifying loop mirror (NALM) and carbon nanotube (CNT) as saturable absorber (SA) [8].

Additionally, multi-wavelength laser sources possessing the advantages of cost-effectiveness, compactness and multi-channel have attracted considerable interests for their wide-spread applications in communication, sensing and spectroscopy. Multi-wavelength lasers at 2 μm have been developed rapidly in recent years. The main difficulty to realize stable multi-wavelength fiber laser is the homogeneous gain broadening of rare earth ions at room temperature. Different approaches have been reported to overcome it. Peng et al. demonstrated a multi-wavelength TDFL based on nonlinear amplifier loop mirror [9]. Wang et al. reported a tunable multi-wavelength TDFL based on polarization rotation and four wave mixing (FWM) effect [10]. Huang et al. reported an all-fiber multi-wavelength TDFL by FWM in highly germania-doped fiber [11]. Liu et al. demonstrated a multi-wavelength TDFL with a highly nonlinear fiber (HNLF) by using nonlinear polarization rotation [12]. All of these laser sources are useful for many applications. However, their relatively large wavelength spacing (from 0.33 nm to 2.5 nm) limits their applications in some specific area,

such as dense wavelength division multiplexing (DWDM). Stimulated Brillouin scattering (SBS) is another way to achieve multi-wavelength operation. It has the advantage of low pump power threshold, narrow linewidth, and small wavelength spacing. For all the above reasons, developing a multi-wavelength Brillouin TDFL at around $2 \mu\text{m}$ is of great significance.

Another notable optical band is the 1600-1800 nm wavelength region, which has drawn wide attention for its potential scientific and practical applications in telecommunication, medicine, sensing, military etc [13]. However, this region contains no wavelengths of efficient rare-earth doped fiber lasers. It was found that bismuth doped germanosilicate glasses can form a luminescence band around 1700 nm [14]. Hence, they cover the wavelength gap between erbium fiber lasers and thulium fiber lasers. Since then, the fibers with this type of glass have been investigated intensively, and such fibers have been successfully used to build and develop broadband optical amplifiers [15], continuous wave (CW) [16] and mode-locked fiber lasers [17] etc.

1.3 Thesis Contribution

In this thesis, we demonstrate a multi-wavelength Brillouin TDFL at 1874 nm. More than 100-wavelength output with uniform wavelength spacing of 0.1 nm has been achieved. A 20 minutes stability test shows the peak powers fluctuate less than 3.4 dB and peak wavelength drift less than 0.02 nm. Such a laser will be important in the fields of telecommunication, spectroscopy, sensing, etc. We also demonstrate a bismuth doped fiber laser (BDFL) at 1726 nm with both linear cavity and ring cavity. The optical spectra and the power relation between input and output powers are shown in this thesis. The bismuth lasers demonstrated in the thesis are of significance for providing new configurations, which could be useful for future researches.

The following is a list of conference papers that have been published or submitted for publication.

C. Jia, J. Qiao, N. Abdukerim, M. Rochette, L. R. Chen. "Multi-wavelength Brillouin Tm³⁺-doped fiber laser at 1873 nm using a linear cavity." *IEEE Photonics Conference*, 2017:281-282.

The idea of this paper was proposed by Prof. Lawrence R. Chen and Dr. Chenglai Jia. The experiments were conducted by Chenglai Jia and me, and all authors contributed to manuscript writing.

G. Nemova, J. Qiao, L. R. Chen, S. V. Firstov, E. M. Dianova. "Dual-wavelength, cascaded cavities bismuth-doped fiber laser in 1.7 μm wavelength range." Submitted to *SPIE Photonics West*, 2018.

The idea of this paper was proposed by Prof. Lawrence R. Chen. Dr. Galina Nemova conducted numerical simulations and I conducted experiments. All authors contributed to manuscript writing.

1.4 Thesis Outline

The thesis is organized as follows. In Chapter 2, some background knowledge of ion doped fibers and fiber optic nonlinearities are introduced first, then this chapter reviews the development of Brillouin fiber lasers and bismuth doped fiber lasers. Chapter 3 demonstrates our multi-wavelength Brillouin Tm³⁺-doped fiber laser with a linear cavity. The configuration of this laser and the optical spectra with different kinds of pumping configurations. At the end of this chapter, the stability of the laser is given by a 5 repeated optical spectra scan in 20 minutes. Chapter 4 demonstrates our CW bismuth doped fiber laser in both linear cavity and ring cavity. The input-output powers relation of the lasers are given and the differences of the results are compared in this chapter. The last Chapter summarizes the work have been done in this thesis, and briefly discusses the future works.

Chapter 2

Background

In this chapter, we first introduce some basic knowledge about ion-doped fibers and fiber lasers. Then some concepts of fiber optic nonlinearities including stimulated Brillouin scattering and four wave mixing are discussed. At the end of this chapter, we review the development of Brillouin fiber lasers and Bismuth doped fiber lasers.

2.1 Ion-doped Fibers

Fiber lasers and fiber amplifiers are based on optical fibers doped with ions. Except in upconversion pumping scheme, these ions absorb pump light at shorter wavelength, and transit into an excited state. This provides conditions for light amplification at longer wavelength by stimulated emission. Such specialty fibers are often called active fibers. Fibers doped with different ions can be used to amplify light at different wavelength.

2.1.1 Tm^{3+} doped fiber

The energy levels of thulium ion (Tm^{3+}) is shown in Fig. 2.1. Tm^{3+} is typically hosted by silicate and germanate glasses or fluoride glasses. In the silicate glass host, transitions through ${}^3\text{F}_4 \rightarrow {}^3\text{H}_6$ are mainly used to generate light around $1.9 \mu\text{m}$. Direct pumping at 1560 nm (${}^3\text{H}_6 \rightarrow {}^3\text{F}_4$) or indirect pumping at 790 nm (${}^3\text{H}_6 \rightarrow {}^3\text{H}_4$) can be used to populate ${}^3\text{F}_4$ level [18]. For the indirect pumping scheme, the rate of the cross relaxation process

${}^3\text{H}_4 + {}^3\text{H}_6 \rightarrow {}^3\text{F}_4 + {}^3\text{F}_4$ is favored by high doping concentration.

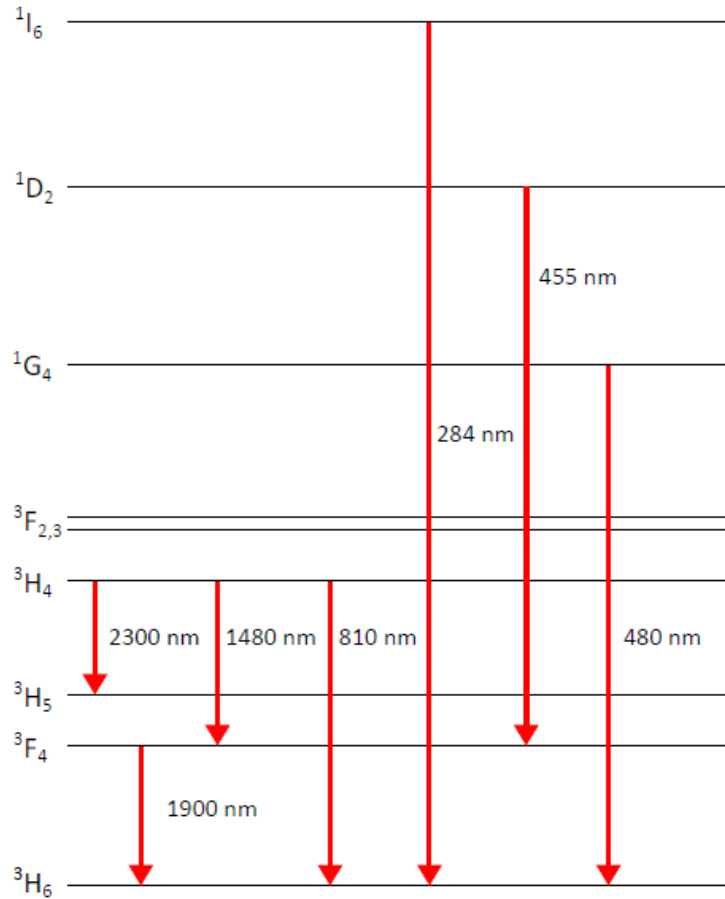


Figure 2.1: Energy-level diagram of the Tm^{3+} ion [19]

In fluoride glass, the lifetime of ${}^3\text{H}_4$ is longer than that of silicate host, which makes it possible to induce lasing through ${}^3\text{H}_4 \rightarrow {}^3\text{H}_5$ (2300 nm), ${}^3\text{H}_4 \rightarrow {}^3\text{F}_4$ (1480 nm), and ${}^3\text{H}_4 \rightarrow {}^3\text{H}_6$ (810 nm). Low Tm^{3+} concentration is preferred in fluoride glass to avoid the cross relaxation process ${}^3\text{H}_4 + {}^3\text{H}_6 \rightarrow {}^3\text{F}_4 + {}^3\text{F}_4$ which depopulates ${}^3\text{H}_4$ level.

2.1.2 Bismuth doped fiber

Unlike the rare earth doped ions, the transition wavelength and energy levels of bismuth ion depends on the host glass [20], because transitions in bismuth active centers (BACs) associate with unshielded outer electron shell. Therefore, varying the composition of host glass can change the wavelength range of luminescence and optical amplification of bismuth

doped fiber. Fig. 2.2 shows the energy levels of Si-BAC and Ge-BAC, respectively. We can see that the energy levels of Si-BAC and Ge-BAC are similar.

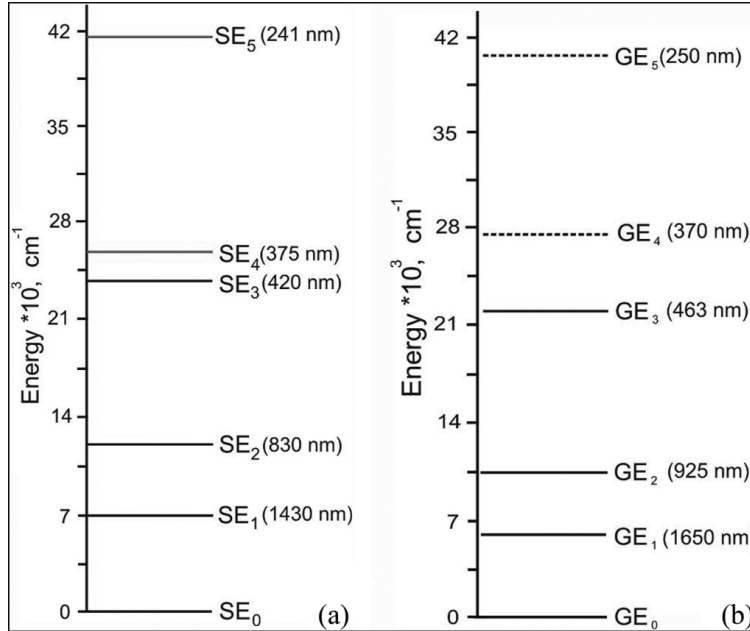


Figure 2.2: Energy-level diagram of (a) Si-BAC and (b) Ge-BAC [20]. ©2014, IEEE

The experimental results show that small doping concentration of GeO_2 does not affect the structure of the Si-BACs. Therefore, it does not change the luminescence peaks and the lifetimes [20]. However, there are two gain bands for Bi-doped high-germania-core fibers in the near infrared range [13]. The first one peaks at around 1400 nm and is produced by the optical transition ($E_1 \rightarrow E_2$) of the Si-BAC. The second one peaks at around 1700 nm and is due to the transition of Ge-BAC. The lifetimes of luminescence are $600 \mu\text{s}$ and $500 \mu\text{s}$, respectively.

Relatively low concentration (typically less than 0.1 wt.%) of bismuth ion is preferred in bismuth doped fibers [21]. When the bismuth ion concentration increases, the concentration of BACs grows in the beginning. However, with a further increase of the bismuth ion concentration, the growth of BAC concentration becomes slower than the growth of background losses, which makes it more and more difficult to achieve optical gain and lasing.

2.2 Fiber Optic Nonlinearities

Similar to the other dielectric materials, when an intense electromagnetic field is applied, the response of optical fiber to the field is nonlinear [22]. The total polarization \mathbf{P} induced from dielectric dipoles satisfies the relation

$$\mathbf{P} = \epsilon_0(\chi^{(1)} \cdot \mathbf{E} + \chi^{(2)} \cdot \mathbf{E}\mathbf{E} + \chi^{(3)} \cdot \mathbf{E}\mathbf{E}\mathbf{E} + \dots) \quad (2.1)$$

where ϵ_0 is the permittivity of vacuum, $\chi^{(j)}$ is the j th order susceptibility and \mathbf{E} is the electric field. Generally speaking, $\chi^{(j)}$ is a $(j + 1)$ th order tensor. The linear susceptibility $\chi^{(1)}$ affects the refractive index n and the attenuation coefficient α . The relation between the linear susceptibility and refractive index is

$$n^2 = \frac{\epsilon}{\epsilon_0} = 1 + \chi^{(1)} \quad (2.2)$$

The second order susceptibility $\chi^{(2)}$ is responsible for the nonlinear effects like second-harmonic generation and sum-frequency generation which are usually generated by nonlinear crystal. However, the second order susceptibility vanishes for silica fiber due to the inversion symmetry of the SiO_2 molecule. Therefore, except some weak second order nonlinear effects exist under certain conditions, there is no second order nonlinear effect in silica fiber.

The third order susceptibility $\chi^{(3)}$ is mainly responsible for nonlinear effects such as third harmonic generation, FWM and nonlinear refraction, which is referring to the intensity dependence of the refractive index and contributes to most of the nonlinear effects in optical fibers, such as self-phase modulation and cross phase modulation. Self phase modulation refers to the phase shift induced by optical field itself during the propagation in fibers and responsible for spectral broadening of ultrashort pulses and generation of optical solitons. Cross phase modulation refers to phase shift induced by another field having different wavelength, polarization state or direction and responsible for asymmetric spectral broadening of copropagating pulses.

The nonlinear effects related to the third order susceptibility $\chi^{(3)}$ are elastic which means there is no energy exchange between electromagnetic field and the dielectric material. A second category of nonlinear effects is inelastic in which electromagnetic field transfers part of its energy to the dielectric material. Two main effects, stimulated Raman scattering and stimulated Brillouin scattering are included in this category. The first one involves optical phonons, while the second one involves acoustic phonons.

2.2.1 Stimulated Brillouin Scattering

SBS effect was first observed in 1964 [23] and has been investigated extensively. The phenomenon of SBS effect is when injecting a signal into the fiber whose power is over Brillouin threshold, a Stokes wave with frequency downshifted will be generated and propagates backward. The process of SBS can be described as a nonlinear interaction among the Brillouin pump and Stokes field and acoustic wave through the process of electrostriction. Electrostriction is a mechanism that the optic fiber materials tend to become compressed with an electric field applied. The temporal spatial density change generates an acoustic wave, and the acoustic wave modulates the refractive index of the optical fiber[24]. This index grating reflects the pump light like a fiber Bragg grating (FBG). Due to the Doppler shift, the backward reflected signal is downshifted in frequency. Because this process must obey energy and momentum conservation rules, we can get the relation

$$\Omega_B = \omega_p - \omega_s, \mathbf{k}_A = \mathbf{k}_p - \mathbf{k}_s \quad (2.3)$$

where ω_p and ω_s are the frequencies, \mathbf{k}_p and \mathbf{k}_s are the wave vectors of the pump and Stokes wave, respectively. Ω_B is the frequency of Brillouin shift, \mathbf{k}_A is the wave vector of the acoustic wave and they satisfy the standard frequency relation

$$\Omega_B = v_A |\mathbf{k}_A| \approx 2v_A |\mathbf{k}_p| \sin(\theta/2) \quad (2.4)$$

where v_A is the velocity of acoustic wave in the fiber, and θ is the angle between the pump and Stokes field. We can see from the Equation 2.4 that the frequency shift depends on

the scattering angle. When the angle is π (backward direction), the frequency shift is maximum, and when the angle is 0 (forward direction), the frequency shift vanishes. In a single mode fiber, there are only two directions, forward and backward, so SBS only occurs in the backward direction with Brillouin shift

$$\nu_B = \Omega_B/2\pi = 2n_p v_A/\lambda_p \quad (2.5)$$

where n_p is the effective mode index at the pump wavelength λ_p , and we use the relation $|\mathbf{k}_p| = 2\pi n_p/\lambda_p$ in the Equation 2.5.

The Brillouin gain spectrum peaks at $\Omega = \Omega_B$, and the spectral width of the gain spectrum is very small. The Brillouin gain has a Lorentzian spectrum [24]

$$g_B(\Omega) = \frac{g_p(\Gamma_B/2)^2}{(\Omega - \Omega_B)^2 + (\Gamma_B/2)^2} \quad (2.6)$$

and the peak value of Brillouin gain is given by

$$g_p = g_B(\Omega_B) = \frac{4\pi^2 \gamma_e^2 f_A}{n_p c \lambda_p^2 \rho_0 v_A \Gamma_B} \quad (2.7)$$

where ρ_0 is material density, γ_e is the electrostrictive constant of fiber, and acoustic waves decay as $\exp(-\Gamma_B t)$. The FWHM of the gain spectrum is related to Γ_B as $\Delta\mu_B = \Gamma_B/(2\pi)$.

Under steady-state conditions, SBS is governed by the following equations when applying a CW or quasi-CW pump [22]

$$\frac{dI_p}{dz} = -g_B I_p I_s - \alpha I_p \quad (2.8)$$

$$\frac{-dI_s}{dz} = g_B I_p I_s - \alpha I_s \quad (2.9)$$

where I_p and I_s are intensities of the Brillouin pump and the Stokes signals, respectively. Two assumptions are used here. First, $\omega_p = \omega_s$ since the Brillouin shift is relatively very small.

Second, $\alpha_p \approx \alpha_s = \alpha$, pump signal and Brillouin signal have almost same attenuations. Equations 2.8 and 2.9 show two facts. Energy is transferred between Brillouin pump signal and Stokes signal, and the signals lose energy during their propagation, which refers to the term $-\alpha I$. The negative sign in front of $\frac{dI_s}{dz}$ is due to the counter-propagating of Stokes wave.

To estimate the Brillouin threshold, replace I_p with $I_p(z) = I_p(0)e^{-\alpha z}$ in Equation 2.9 and do the integration over length L, we can get

$$I_s(0) = I_s(L) \exp(g_B P_0 L_{eff} / A_{eff} - \alpha L) \quad (2.10)$$

where $P_0 = I_p(0)A_{eff}$ is the input pump power, A_{eff} is the effective mode area and L_{eff} is the effective length which is defined by $L_{eff} = \frac{1 - \exp(-\alpha L)}{\alpha}$. The Brillouin threshold power is defined as the input pump power at which the Stokes power equals to the pump power at the fiber input. Therefore, we can find the estimated Brillouin threshold power P_{th} by the relation

$$g_B(\Omega_B) P_{th} L_{eff} / A_{eff} \approx 21 \quad (2.11)$$

The length of the fiber plays an important role in Brillouin signal generation.

2.2.2 Four Wave Mixing

The FWM effect is a nonlinear effect refers to the third order susceptibility $\chi^{(3)}$. FWM in optical fiber was investigated as soon as low loss fibers was demonstrated for the first time [25]. There are two types of FWM, see Fig. 2.3. The first one is called non-degenerate FWM. It can happen if more than two signals with different frequencies propagate together in an optical fiber. When launch two pump signals with carrier frequencies ν_1 and ν_2 , a refractive index modulation occurs and two new signals with frequencies of ν_3 and ν_4 are generated. Their frequencies relation can be described by

$$\nu_3 + \nu_4 = \nu_1 + \nu_2 \quad (2.12)$$

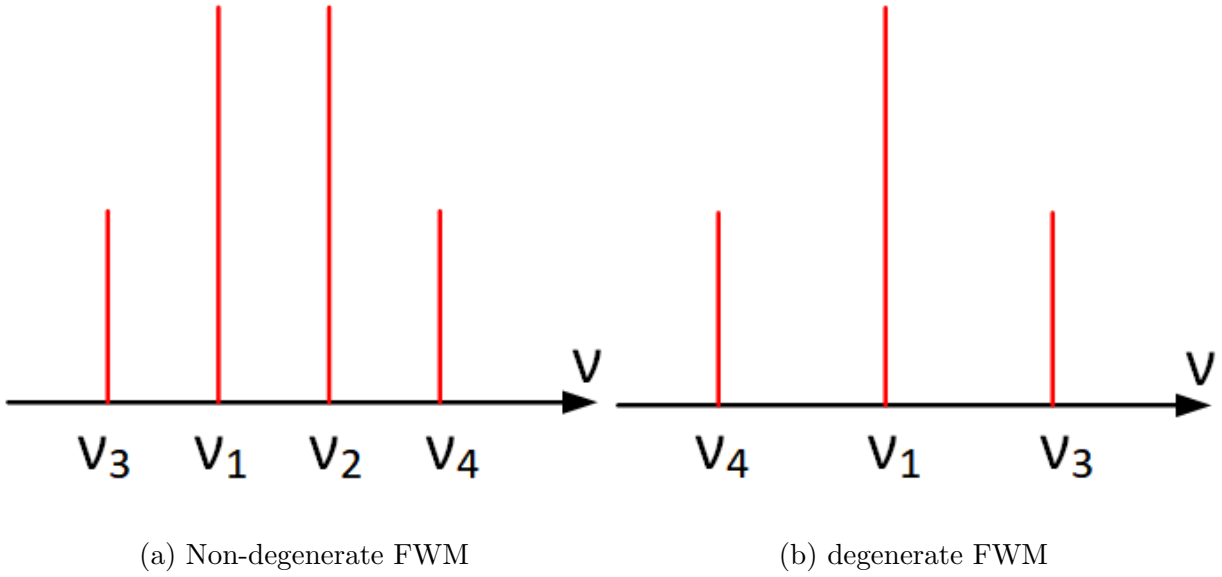


Figure 2.3: Generation of new signals with ν_3 and ν_4 via FWM

The other type of FWM is called degenerate FWM. It is a special case when $\nu_1 = \nu_2$. We have the relation

$$2\nu_1 = \nu_3 + \nu_4 \quad (2.13)$$

A strong pump signal at ν_1 creates two new signals located symmetrically at ν_3 and ν_4 which are referred to Stokes and anti-Stokes signal, respectively.

FWM is a phase sensitive process. Only if a phase-matching condition is satisfied, the effect can accumulate over long distance. The phase matching condition is

$$\Delta k = (\bar{n}_3\omega_3 + \bar{n}_4\omega_4 - \bar{n}_1\omega_1 - \bar{n}_2\omega_2)/c = 0 \quad (2.14)$$

where \bar{n}_j is the effective mode index at the frequency ω_j . Otherwise, the FWM is strongly suppressed if there is a large phase mismatch.

2.3 Review of Previous work

2.3.1 Review of Brillouin Fiber Lasers

The Brillouin fiber laser was initially realized with erbium doped fiber laser (EDFL) at around $1.55 \mu\text{m}$. In 1996, Gregory J. Cowle and Dmitrii Yu. Stepanov demonstrated the first Brillouin EDFL [26] shown in Fig. 2.4 (a). The idea of the laser was to inject a high power Brillouin pump (BP) signal into a ring cavity generating a 10.35GHz (equivalent to 0.08 nm) shifted Stokes signal. As we introduced in Chapter 2, this is due to the Doppler shift, and the Brillouin shift can be estimated by the Equation 2.5. The generated Brillouin signal was then amplified by an EDFA pumped with a 980 nm source. After this work, they developed the ring cavity to allow multi-wavelength operation [27], which is shown in Fig. 2.4 (b). They added an extra SMF into the ring cavity, which allowed the generated Stokes signals re-inject into the cavity, generating cascade Stokes signals and realizing multi-wavelength operation. This laser generated 5 lasing peaks with 10 GHz line spacing.

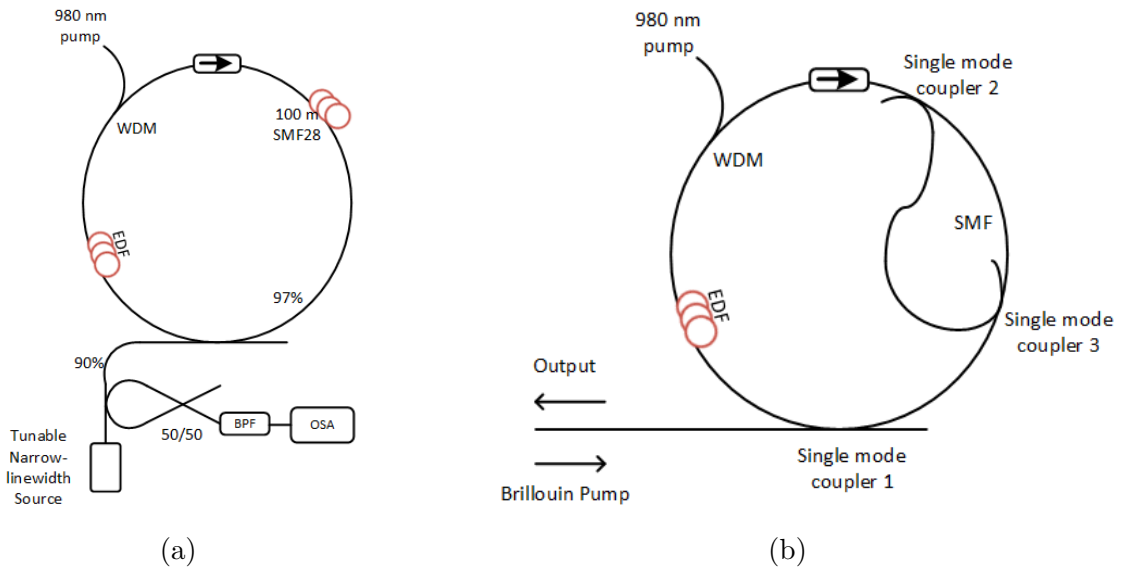


Figure 2.4: Experimental laser configurations for (a) the first Brillouin EDFL and (b) the first multiple wavelength Brillouin EDFL.

Following this work, there have been several improvements in Brillouin EDFL. Nam Seong Kim added an EDFA in the feedback path to enhance the Brillouin signals. a four-line output of 1532.00, 1532.08, 1532.17 and 1532.27 nm was obtained with 1531.91 nm Brillouin

pump. They also investigated the threshold behaviors and confirmed that Brillouin pump can control the number of lasing lines. The laser setup is shown in Fig. 2.5.

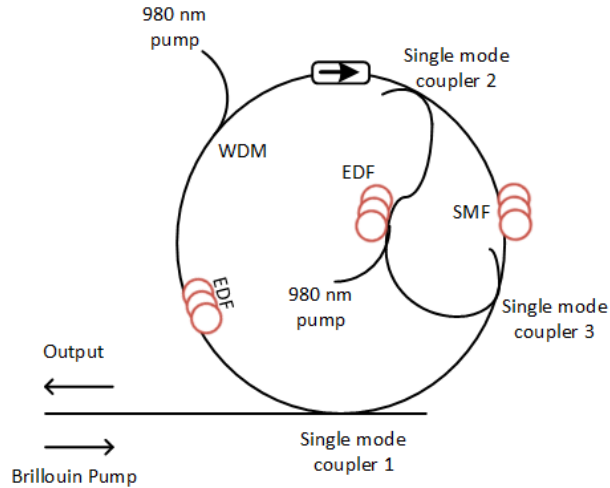


Figure 2.5: Schematic diagram of the EDFA-enhanced Brillouin EDFL

In 2000, Park et al. demonstrated a Brillouin EDFL generating multi-wavelength operation shown as Fig. 2.6 [28]. They used a circulator to give feedback into the cavity. Two EDFAs were used to amplify the signals in the cavity and feedback path. This laser could generate a 53-line output.

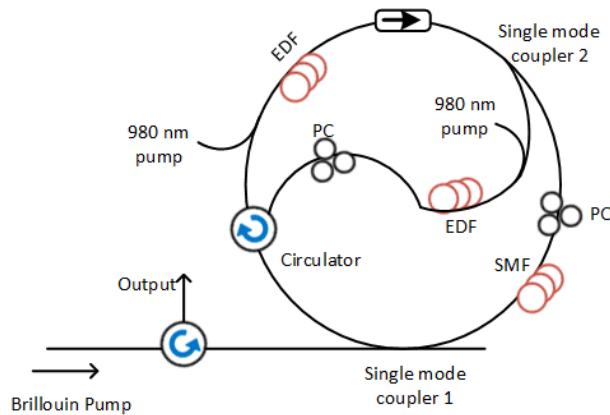


Figure 2.6: Schematic diagram of BEFL with internal feedback

In 2005, a new design of multi-wavelength Brillouin EDFL with a linear cavity was demonstrated for the first time by Al-Mansoori et al. [29]. The laser configuration was shown in Fig. 2.7. Two circulators (Cir 2 and Cir 3) were used to form two loop mirrors.

The linear cavity was defined by these two loop mirrors. The Brillouin gain medium was a 1.9 km long SMF-28 pumped by BP via a 3dB coupler and another circular (Cir 1) with the output extracted by the same coupler and circulator from the laser cavity. A 22-lines output operation with spacing of 10.88 GHz was achieved at 1557.5 nm. To get a stable multi-wavelength operation, they optimized the BP power and EDF pump power to suppress the free running modes of EDFL.

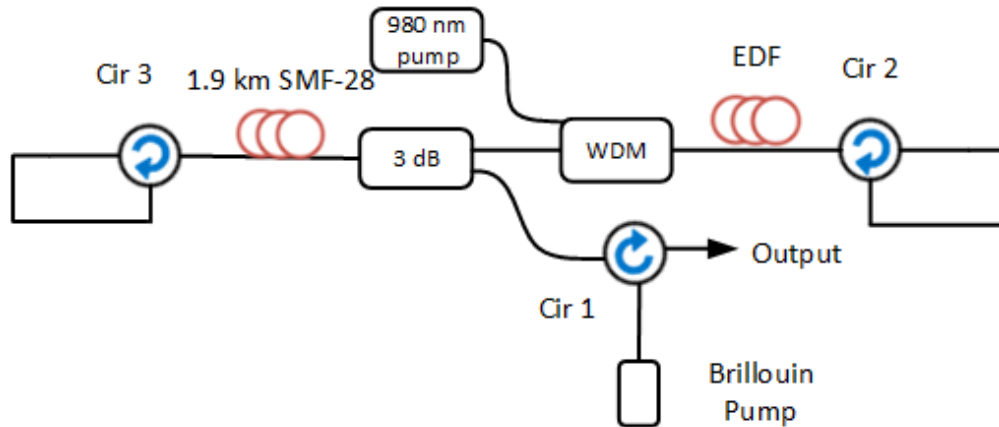


Figure 2.7: Configuration of the first Brillouin EDFL with a linear cavity

In 2014, Wang et al. reported the first multi-wavelength Brillouin thulium doped fiber laser [30]. The laser setup is shown in Fig. 2.8. A typical inverse S-shaped configuration is used in the ring cavity to generate multi-wavelength. A 450 m long SMF28 was used as the nonlinear medium. The BP power was a single frequency fiber laser with linewidth of less than 100 kHz and wavelength of $1.97 \mu\text{m}$. This BP laser was then pumped by a TDFA composed by a 7 m long double cladding Tm-doped fiber and two 793 nm laser diodes. Five Stokes lines with 0.105 nm spacing were observed in the output optical spectrum. In a 20 minutes test, the 5 peak powers fluctuated less than 0.5 dB, and peak wavelengths shifted less than 0.01 nm.

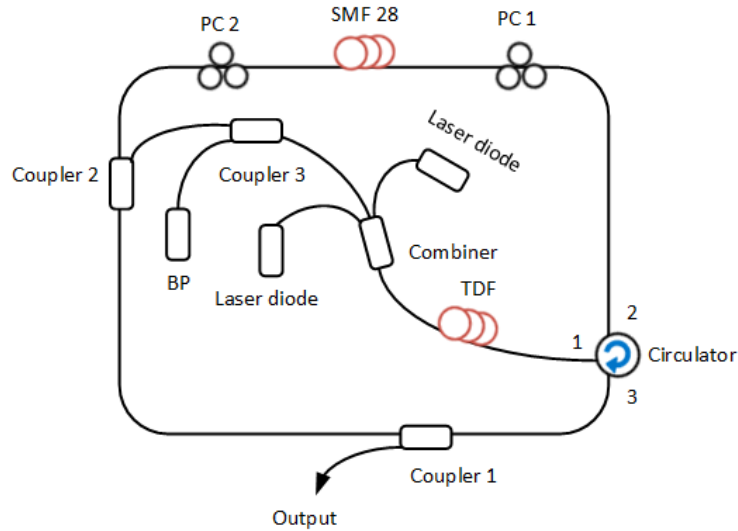


Figure 2.8: Setup of the multiwavelength Brillouin TDFL

Besides the multi-wavelength fiber laser, the SBS effect was also used to generate narrow linewidth fiber laser. In 2014, Luo et al. demonstrated the first high optical signal to noise ratio (OSNR) single frequency $2\ \mu\text{m}$ Brillouin TDFL with watt-level output and high transfer efficiency [31], which is shown in Fig. 2.9. A fiber-coupled $2\ \mu\text{m}$ DFB laser with linewidth less than 1 MHz and output power of 2 mW worked as pump signal. Before coupled into the first ring cavity, the pump signal was amplified by two TDFAs. After the second TDF, the pump signal could be up to 4.02 W. The first ring cavity had an optimum length of 14 m to generate the Brillouin signal. To measure the linewidth of the generated Brillouin signal, they coupled the signal into a second ring cavity to generate second Brillouin signal. The beating between the first and second Brillouin signals reveals the linewidth of the first Brillouin fiber laser. Since the linewidth of the Brillouin signal is much narrower than Brillouin pump [32], the output signal could be narrowed to 8 kHz from 1 MHz. The transfer efficiency of the laser is 51% with 1.08 W output power and 62 dB OSNR for 3.22 W pump power.

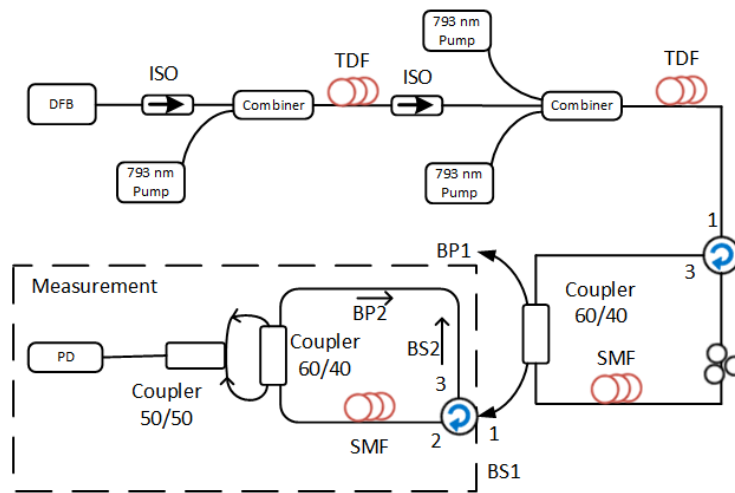


Figure 2.9: Experimental configuration of the high signal to noise ratio, signal-frequency 2 μm Brillouin fiber laser

In 2017, Fu et al. demonstrated a linewidth-narrowed, linear-polarized, single-frequency TDFL based on SBS effect [33]. The setup is shown in Fig. 2.10. A TDFL with an output power of 25 mW and a linewidth of 36 kHz was pre-amplified through a TDFA to serve as a BP signal. The amplified BP signal was then injected into a ring cavity. A 10 m TDF pumped by a 793 nm laser diode was used to amplify both BP and the generated Stokes signal. A 10 m long polarization maintaining fiber (PM-1550) was added into the ring cavity to decrease the Brillouin threshold. The output signal had a frequency down-shift of 8.34 GHz from BP and a linewidth of only 4.6 kHz, which is 8 times narrowed compared to the BP.

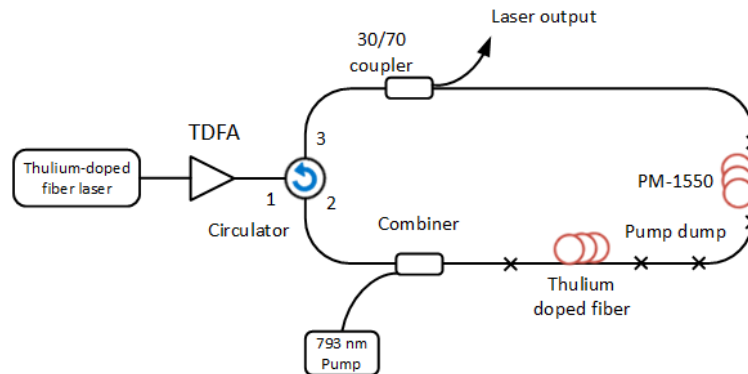


Figure 2.10: Experimental setup of the Hybrid Brillouin-thulium single-frequency fiber laser

2.3.2 Review of Bismuth Doped fiber laser

Rare earth doped fiber lasers in the wavelength region of near-IR have been widely used. However, there is no efficient rare earth doped fiber laser within the region of 1150-1500 nm and 1600-1800 nm. Due to the applications like advanced communication, medicine can be used in these wavelength regions, there is a great demand for new fiber lasers and amplifications in these spectral regions. In 2001, Yasushi Fujimoto and Masahiro Nakatsuka discovered a new infrared luminescence from bismuth doped silica fiber [34]. The luminescence band at 1250 nm with a bandwidth of 300 nm makes it possible to construct a BDFL in 1150-1550 nm region.

The first BDFL was proposed in 2005. Dianov et al. reported the the fabrication of bismuth-doped fibers by the method of chemical vapour deposition (MCVD) and proposed the first CW BDFL [35] with both linear cavity and ring cavity. The fibers were doped with low bismuth concentration ($<0.1\%$), and show absorption bands at 500, 700, 800 and 1000 nm, and emission band at 1150 nm with a full width at half maximum (FWHM) of 150 nm. The scheme of the linear laser is shown in Fig. 2.11, the laser was pumped by a 1064 nm Nd:YAG laser. The linear cavity was defined by a pair of FBGs. The output wavelength was determined by the choice of FBGs, the lasing at 1146, 1215, 1250 and 1300 nm was obtained. After the optimization of the losses, the slope efficiency of this laser can achieve 0.3 W/W.

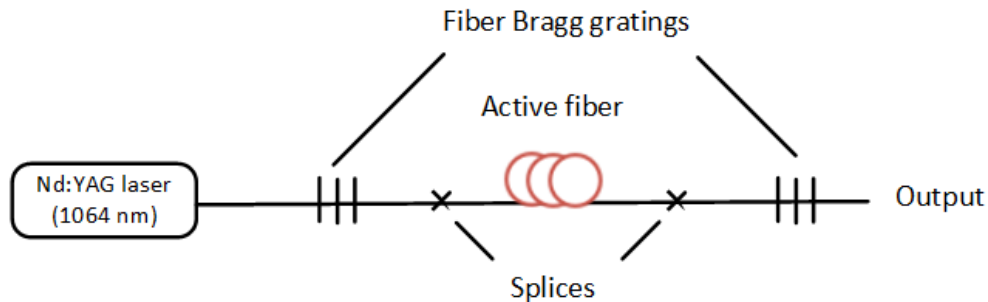


Figure 2.11: Experimental setup of the first BDFL with linear cavity

The scheme of the first ring cavity BDFL is shown in Fig. 2.12, the laser was pumped by the same Nd:YAG laser. An optical coupler was used to form a ring cavity. The coupling

coefficient of the resonator was less than 20% in the wavelength of 1.1-1.2 μm . The optical spectra of this laser showed that there were many longitudinal modes due to a weak selectivity of the resonator when the pump power was slightly above the threshold power. As the pump power increased, the number of peaks reduced. When the pump power exceeded the threshold considerably, only one peak at 1172 nm remained.

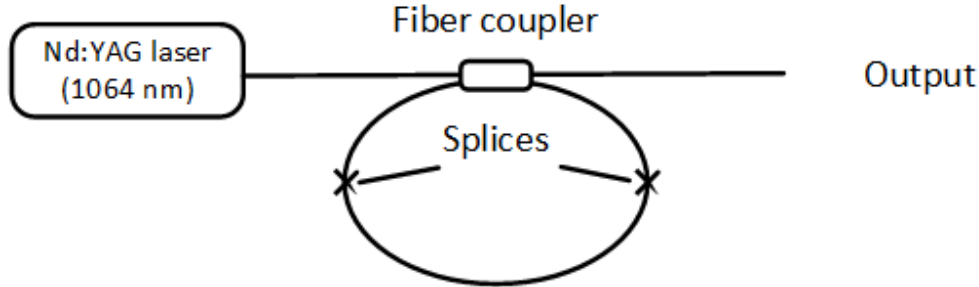


Figure 2.12: Experimental setup of the first BDFL with ring cavity

Following this work, there have been several developments in BDFL. In 2007, Dianov et al. demonstrated a high power CW BDFL in the wavelength range of 1150-1215 nm for the first time [36]. The scheme of the experiment is shown in Fig. 2.13. A CW Yb fiber laser was used as pump source. The output power of this pump was up to 80 W at the wavelength of 1070 nm. 83 meters long bismuth doped aluminosilicate glass fiber with bismuth concentration of $1.3 * 10^{19} \text{cm}^{-3}$ was used as active fiber in the laser. The output power of this BDFL was up to 15 W. In this work, they also measured the unbleachable losses of Bi-doped fibers, investigated the temperature dependence of these losses, and demonstrated the yellow-light generation by using the BDFL with frequency doubling. At the end of this paper, they pointed out that the main problems of BDFL at that time were large unbleachable losses and low concentration of bismuth ions in the fiber core, which provides a guidance for the future works.

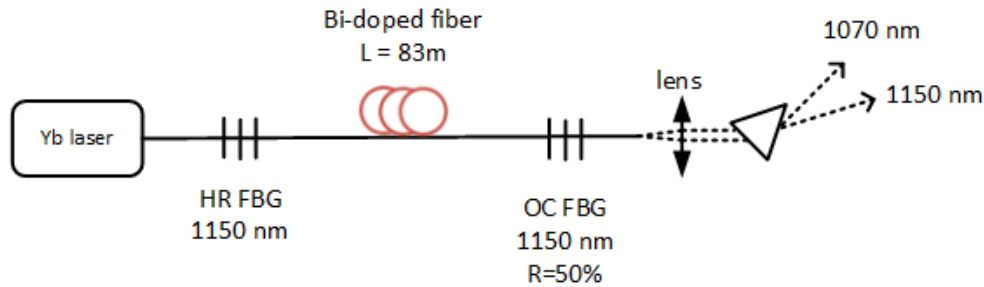


Figure 2.13: Experimental setup of the CW high power BDFL

The first mode-locked bismuth doped fiber laser was reported in 2007 by Dianov et al. [37]. The experimental setup was shown in Fig. 2.14. The active fiber was a 6 m long bismuth-doped silicate glass fiber, and the bismuth concentration was around 0.02%. The fiber was pumped by a 800 mW 1063.8 nm cw Yb fiber laser through a 1065/1160 nm WDM coupler. The laser cavity was defined by a high reflectivity FBG and a SESAM. The SESAM based on GaInNAs was optimized for 1100-1200 nm wavelength range. The average power of this laser was 2 mW, and the single pulse width was 50 ps for 2 MHz repetition rate. The laser emitted the linewidth of 0.02 nm at 1161.6 nm.

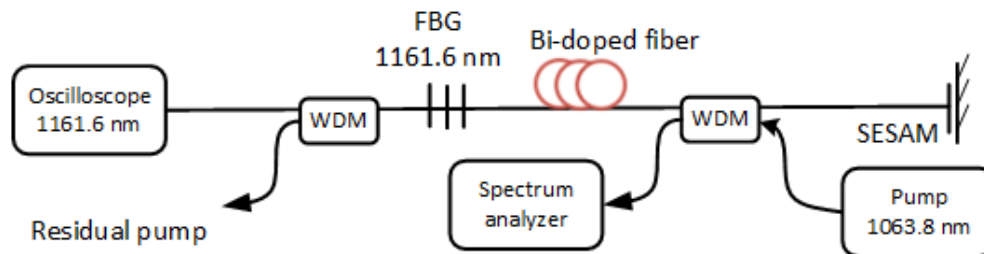


Figure 2.14: Mode-locked Bi-doped fiber laser configuration

Besides the 1150-1550 nm wavelength region, it was found that bismuth incorporated in a germanosilicate glass can form a luminescence band around 1700 nm. Since then, such fibers have been used to develop fiber lasers in the wavelength region of 1600-1800 nm.

In 2014, the first bismuth-doped lasers operating in 1625-1775 nm have been developed for the first time by Alyshev et al. [38]. The active fiber was a bismuth doped germanosilicate fiber with ≈ 50 mol.% GeO_2 content and bismuth concentration of 0.1 mol.%. This fiber was fabricated by MCVD technique. The fiber laser was constructed by a common

linear cavity, which consists of the active fiber and a couple of FBGs. The couple of FBGs determined the output wavelength. This laser was pumped by a Er-Yb doped fiber laser operating at 1568 nm, and the pump radiation was launched into the core of the bismuth doped fiber. A laser operation at 1703 nm with a slope efficiency of 20% was achieved.

In 2015, Alyshev et al. demonstrated a watt-level CW bismuth doped fiber laser at $1.7 \mu\text{m}$ [16]. The configuration is shown in Fig. 2.15. The core glass of the active fiber was composed of $50\text{GeO}_2\text{-}50\text{SiO}_2$ with total bismuth concentration of 170 ppm. This fiber was pump by a $\text{Er}^{3+}/\text{Yb}^{3+}$ codoped fiber laser at 1568 nm, which was pumped by a semiconductor laser diodes at the wavelength of 915 nm. The $\text{Er}^{3+}/\text{Yb}^{3+}$ fiber laser cavity was formed by a high reflectivity FBG and a 10% output coupler FBG. The BDFL cavity was composed by a high reflectivity FBG and an output coupler FBG. Different lengths of BDF were tested as gain medium and different FBGs were tested as output coupler in their work. It was found that the maximum slope efficiency of 33% was achieved for a fiber length of 25 m and output coupler of 4%. The output power of this BDFL was be up to 1.05 W.

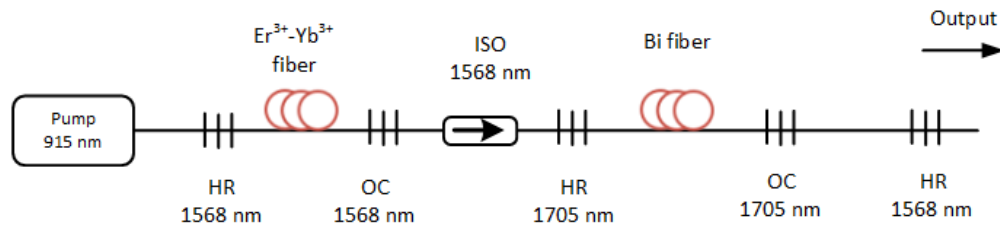


Figure 2.15: High power BDFL configuration at $1.7 \mu\text{m}$

In 2016, Firstov et al. demonstrated the first mode-locked bismuth-doped fiber laser operating at $1.7 \mu\text{m}$ [17]. The laser scheme is shown in Fig. 2.16. The active fiber was a bismuth doped germanosilicate fiber with equal content of GeO_2 and SiO_2 . The fiber core has a bismuth concentration of 0.02 wt.%. A CW EDFL was used as pump source. The pump signal at 1565 nm was launched into the cavity by a dichroic 1560/1730 WDM coupler. The laser cavity was defined by a SA with two layers of CNT and a loop mirror, which directed 35% of the signal to the output. The SMF-28 fiber was used to manage the total dispersion of the cavity. Pulse operation was demonstrated in their work for the laser cavity with both

anomalous and normal dispersion. The laser delivered 1.65 ps pulses in anomalous dispersion regime and 14 ps in normal dispersion regime which could be compressed to 1.2 ps by adding SMF-28 to the output of the laser.

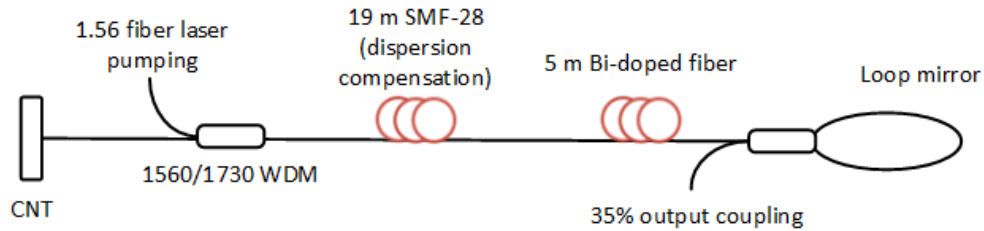


Figure 2.16: The schematic of the mode-locked bismuth fiber laser operating in the anomalous dispersion regime

Another mode-locked BDFL was demonstrated in 2018 by Khagai et al. [39]. Fig. 2.17 shows the experimental setup of the laser. The gain medium of the laser was a 15 m long active bismuth doped germanium silicate fiber with 50 mol. % of GeO_2 . To increase the Kerr nonlinearity effect, a 25 m long germanosilicate fiber with 30 mol. % of GeO_2 was used to manage the dispersion. As a result, single pulse lasing with 4.7 W peak power and 87 pJ pulse energy was realized. The average power of the signal was 0.3 mW. This laser had a pulse duration of 17 ps with repetition rate of 3.57 MHz. The pulse duration can be compressed to 630 fs by using a 150 m long SMF-28.

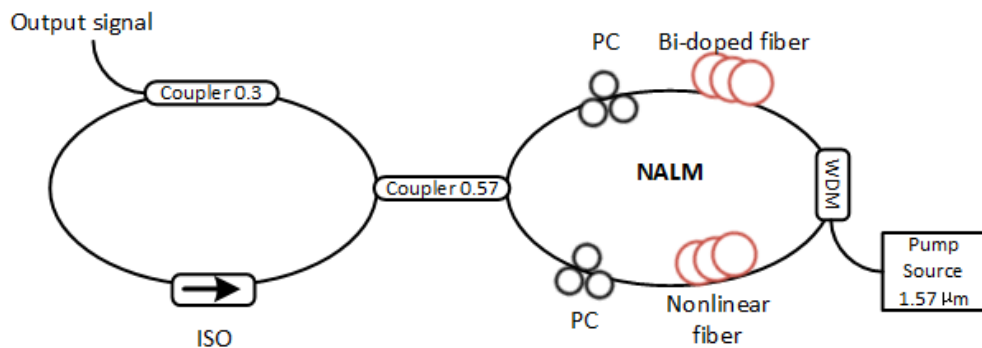


Figure 2.17: Schematic of the NALM-based BDFL at 1.7 μm

2.4 Summary

In this chapter, we reviewed some basics of fiber optics. The ion-doped fibers including Tm^{3+} doped fiber and bismuth doped fiber were introduced. Then, the fiber optic nonlinearities focused on SBS and FWM effects was discussed. Finally, the development of Brillouin fiber lasers and bismuth doped fiber lasers were reviewed.

Chapter 3

Multi-Wavelength Brillouin

Tm³⁺-Doped Fiber Laser at 1874nm

3.1 Introduction

In the 2017 IEEE Photonic Conference, we demonstrated a multi-wavelength Brillouin TDFL using a 2 km SMF-28 with linear cavity [40]. Five Brillouin peaks can be observed in its output spectrum. Its peak powers fluctuate less than 0.5 dB and wavelengths shift less than 0.01 nm. such a laser can be utilized in the area of telecommunications, atmospheric spectroscopy and coherent LIDAR. However, the number of lasing wavelength is still not enough for some specific application like DWDM. Therefore, we improve the laser by using highly nonlinear fiber (NLNF) instead of SMF-28 and replace one gold-tipped mirror with a loop mirror.

In this chapter, we demonstrate a multi-wavelength Brillouin TDFL at 1874 nm with a linear cavity using a 1 km HNLF as Brillouin gain medium due to its high nonlinear coefficient. The Tm³⁺-doped fiber and some home-built devices are introduced first. The setup of the laser is demonstrated later. The results and some phenomena occurred in the experiments are discussed at the end of the chapter.

3.2 Tm³⁺ Doped Fiber

In our laser setup, a Tm³⁺-doped DC silica fiber is used as gain medium. The thulium fiber has a doping concentration of 40,000 ppm Tm³⁺ ions, an 6 μm core diameter with a core numerical aperture (NA) of 0.23, a 125 μm cladding diameter with a cladding NA larger than 0.45. The fiber is coated with 67.5 μm of acrylate and spliced with SMF-28 fiber connectors. The fusion splicing loss is around 0.9 dB per pair due to the mode field diameter mismatch. To build a TDFL, it is necessary to know the amplified spontaneous emission (ASE) spectra of the fiber we are using. The setups of the forward and backward ASE measurement of the Tm³⁺-doped silica fiber are shown in Fig. 3.1(a) and (b), respectively. The 1560 nm pump source is made up of a external cavity laser diode (ECL) and a high power EDFA (PriTel, FA-33) with a maximum output power of 2.3 W. In the forward pump setup (Fig. 3.1(a)), the pump source is connected to the 25 cm Tm³⁺-doped silica fiber directly, and the cross points represent fusion splices. An optical spectrum analyzer (OSA, YOKOGAWA, AQ6375) is connected to the 1900 nm port of 1560/1900 nm WDM coupler for ASE measurement, while, the residual 1560 nm pump signal is coupled into the 1560 nm port. This design is to protect the OSA. In the backward pump setup (Fig. 3.1(b)), the pump source is connected to the 1560 nm port of WDM coupler, and then coupled into Tm³⁺-doped fiber. The ASE results are measured by the same OSA.

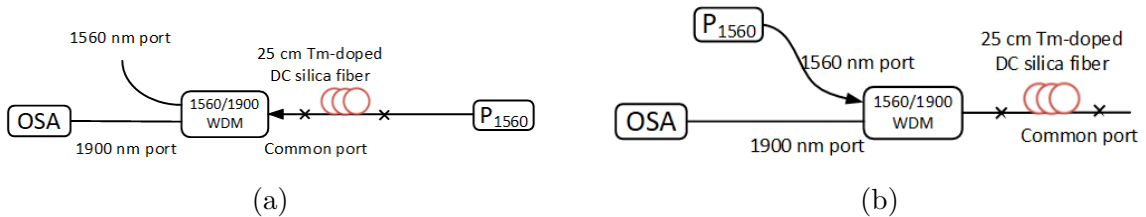


Figure 3.1: Experimental setup to measure Tm³⁺:silica fiber ASE with (a) forward pump and (b) backward pump

The ASE measurement results with forward and backward pump are shown in Fig. 3.2. The 25 cm thulium-doped fiber is pumped by 100 mW, 300 mW, 500 mW, 700 mW, 1 W and 1.4 W, respectively. The pump power is measured by the power meter (Thorlabs, S302C) along with a thermal sensor (Thorlabs, PM1000D) with a resolution of 1 μW . From the

results, we can see that both forward ASE and backward ASE increase with pump power increase. The forward ASE peaks move from 1920 nm to 1870 nm with pump power increase, while the backward ASE peaks remain unchanged at around 1870 nm. The forward ASE spectra have a FWHM bandwidth of around 90 nm from 1816 nm to 1905 nm, and the backward ASE spectra have a FWHM bandwidth of around 90 nm from 1833 nm to 1923 nm. It is noted that forward ASE spectra is higher when wavelength is larger than 1800 nm with the same pump power, which means the Tm^{3+} -doped silica fiber can provide higher gain with forward pumping scheme. Therefore, the forward pumping scheme is used in our laser.

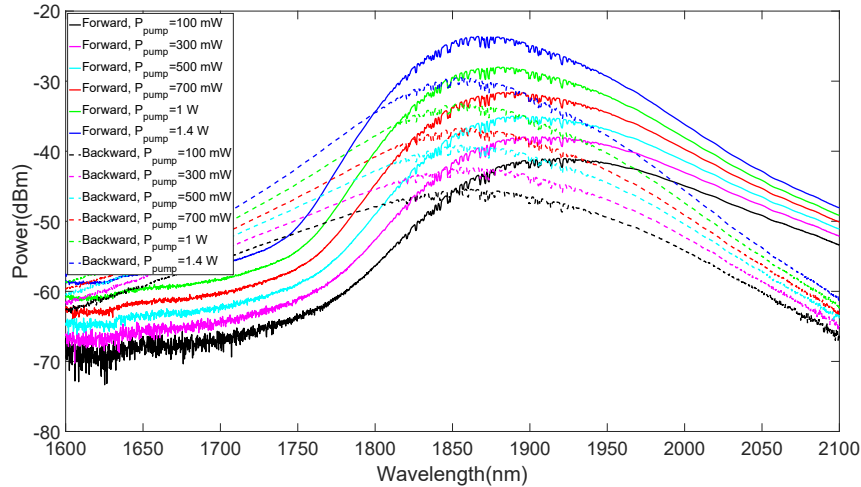


Figure 3.2: Measured ASE spectra of 25 cm Tm^{3+} -doped silica fiber with forward pump and backward pump

To find the optimal length of Tm^{3+} -doped silica fiber for gain medium, we measured ASE spectra with different lengths of fiber under a 2 W forward pump power. Fig. 3.3 shows the results. We can observe that as the length increases, the forward ASE peak moves to longer wavelength, and the ASE output increase first (from 10 cm to 25 cm) and then decrease (from 25 cm to 95 cm). The 25 cm Tm^{3+} -doped silica fiber has the highest ASE output at 1874 nm. Therefore, the 25 cm Tm^{3+} -doped silica fiber is chosen in our laser.

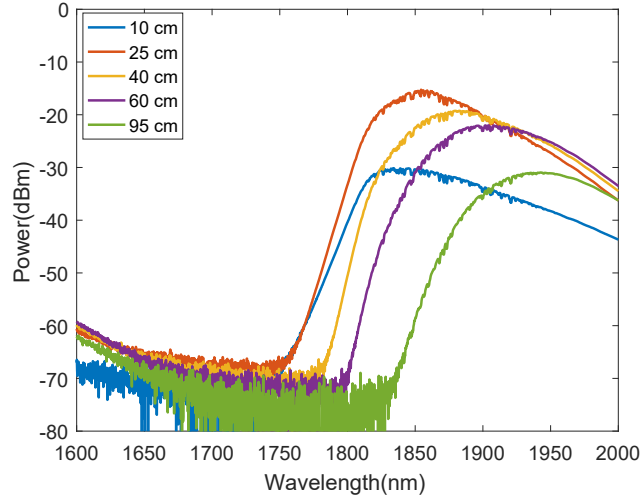


Figure 3.3: Measured ASE spectra with different lengths of Tm^{3+} -doped fiber under a 2 W forward pump power

3.3 Experimental Setup and Results

3.3.1 Brillouin Pump Laser

The Brillouin TDFL is pumped by a home-built TDFL. In this section, we demonstrate the pump laser in a ring cavity. As we introduced earlier, the threshold power of SBS is related to the linewidth of the pump signal. To lower the threshold of stimulated Brillouin scattering and stabilize the output of the multi-wavelength Brillouin TDFL, we tried to build a single longitudinal mode (SLM) laser at 1874 nm as Brillouin pump source. The experimental setup of the Brillouin pump laser is shown in Fig. 3.4(a). An external cavity laser (ECL, P_{1560}) diode is used as the pump source which is passed through an high power EDFA for higher pump power. The pump power can be up to 2.3 W. The WDM coupler (1560/1900 WDM) is used to separate the pump and the lasing signals. The details of double cladding Tm^{3+} -doped silica fiber is introduced in the last section. An in-line polarization controller (PC) ensures the intra-cavity polarization state is properly controlled. A polarization dependent isolator (PDI) is used for suppressing mode competition [41]. A circulator combined with a FBG serve as an isolator and a wavelength selector. The circulator make the lasing signal propagate clockwise. The FBG has a center wavelength of 1873.9 nm, a

3-dB bandwidth of 0.2 nm and a reflectivity of 98%. The residual 1560 nm pump signal is removed from it, and only 1873.9 nm signal can oscillate in this ring cavity. To realize the SLM operation, two compound rings and an unpumped Tm^{3+} -doped fiber are incorporated into the setup. The compound rings serve as highly mode-selective elements. The incommensurate lengths of the compound rings produce the vernier-type effect. Therefore, the laser mode oscillates only at a frequency that satisfies both resonant conditions given by main cavity and two ring cavities [42]. A PC is used in the first compound ring to adjust the polarization state. The length of the two compound rings are 6.8 m and 2.3 m, respectively. The unpumped Tm^{3+} -doped fiber is incorporated into the second ring cavity. This unpumped length, in which a weak Bragg grating is induced due to refractive index changes, allows for SLM operation[43]. Since the residual pump signal is blocked by circulator, it is ensured the the SA in the compound ring is unpumped. A 3 dB coupler extract the 50% intra-cavity power as output power. The total cavity length of this ring cavity is around 16.1 m, and the estimated cavity loss is about 14 dB.

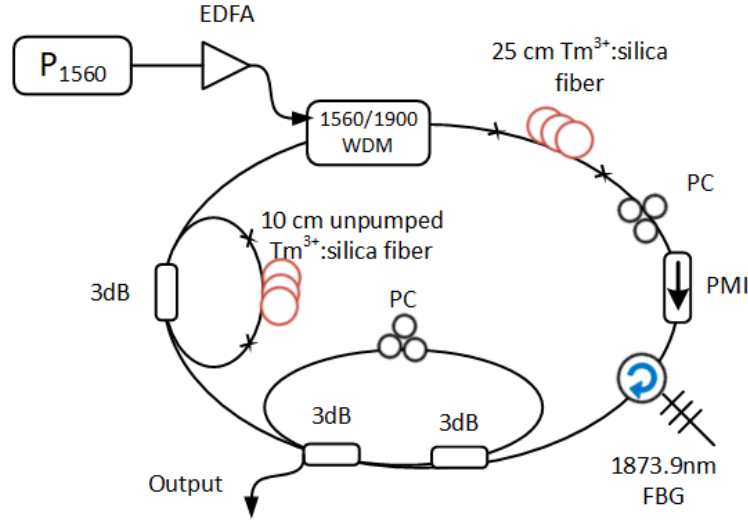


Figure 3.4: Setup of Brillouin pump laser with compound rings and saturable absorber

The output power is connected to a 7.5 GHz photodetector (Newport, 818-BB-51F) and an electrical spectrum analyzer (ESA, Anritsu, MS2668C) to measure its radio frequency (RF) spectrum. The measured RF spectra of the Brillouin pump laser are shown in Fig. 3.5. We can see that all the sidemodes are eliminated by the compound rings and SA, and

only the main lasing mode appears in the RF spectrum, which verifies the single longitudinal operation operation.

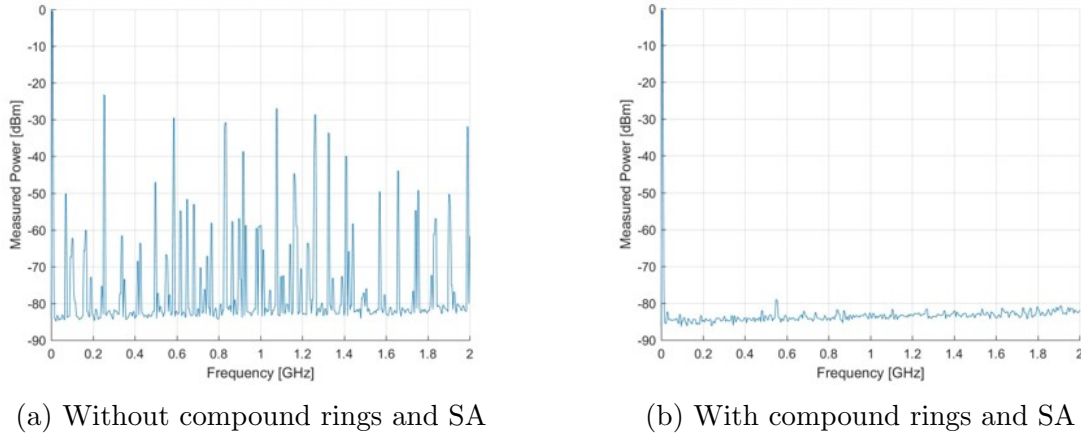


Figure 3.5: The measured RF spectra of the Brillouin pump laser

Fig. 3.6(a) shows the optical spectrum of the Brillouin pump laser. The output spectrum is measured by an OSA (YOKOGAWA, AQ6375) with a resolution of 0.05 nm. The laser peaks at 1873.9 nm and its measured FWHM bandwidth is smaller than 0.06 nm, which is limited by the resolution of the OSA. Fig. 3.6(b) shows the measured output power of the 1873.9 nm with respect to the pump power at 1560 nm. The threshold pump power of the laser is around 0.8 W. When the pump power increases, the laser peak at 1873.9 increases with a slope efficiency of 1.1%.

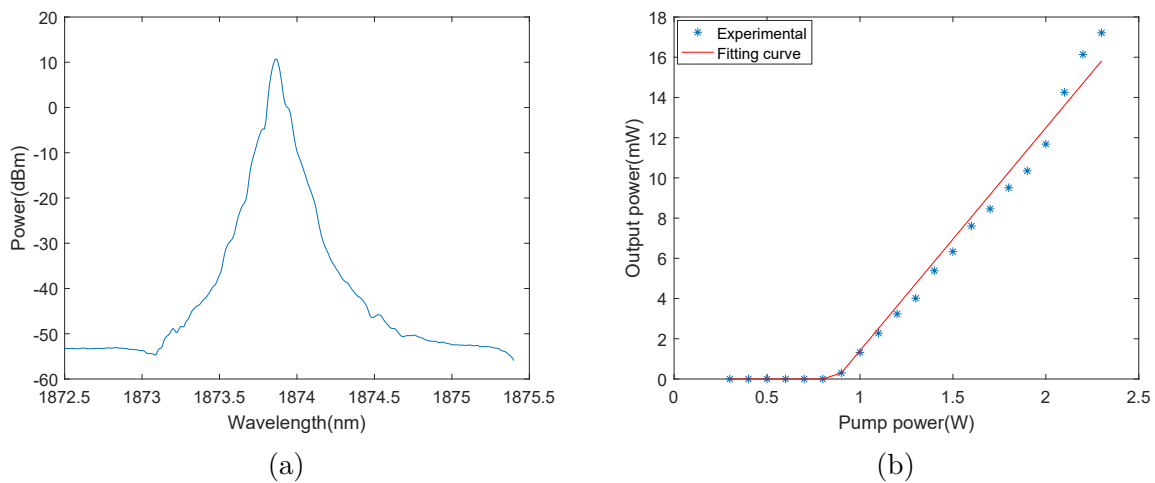


Figure 3.6: (a) The optical spectrum of the Brillouin pump laser. (b) The output power of 1873.9 nm versus pump power at 1560 nm

To test the stability of this BP laser, we measured the optical spectra of this laser 5 times in 20 minutes. The results are shown in Fig. 3.7. The output power fluctuation is less than 0.8 dB, and the wavelength drift is less than 0.1 nm.

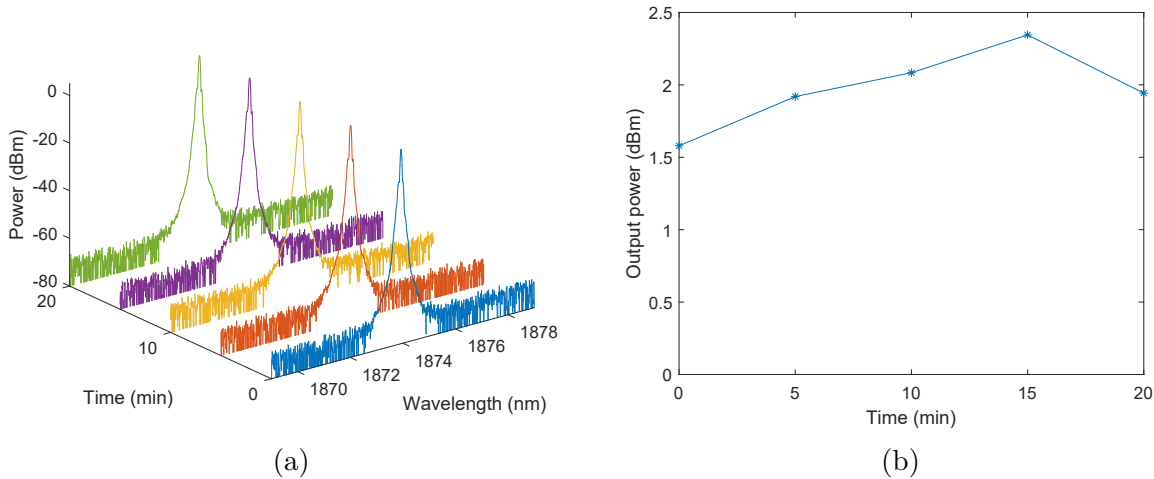


Figure 3.7: (a) optical spectra measured in 20 minutes, (b) output power fluctuation in 20 minutes

3.3.2 Home-Built Thulium Doped Fiber Amplifier

In our Brillouin TDFL setup, there are two home-built thulium doped fiber amplifiers (TDFA). One is used to amplify the 1874 nm pump signal from the Brillouin pump laser and composed of the Brillouin pump (BP) source. The other one is an intra-cavity TDFA to amplify both pump signal and Brillouin signals. In this section, we demonstrate the home-built TDFA. The setup of TDFA is shown in Fig. 3.8. A high power EDFA is used as pump source. The output power of this EDFA can be up to 1.4 W. A 1550/1850 WDM coupler is used to separate the pump and input signal. A 38 cm Tm^{3+} -doped DC silica fiber works as gain medium. This fiber has the same characters as the gain fiber in home-built SLM fiber laser. It is pumped by backward pumping scheme to eliminate the 1550 pump signal in output signal. It is noted that there is no isolator in our home-built TDFA, because we need it work in the linear cavity of Brillouin TDFL.

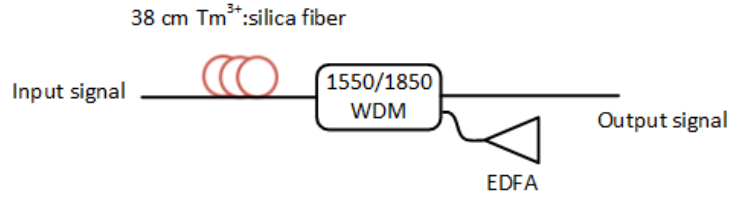


Figure 3.8: Setup of thulium doped fiber amplifier

Fig. 3.9 shows the experimental setup to measure the gain of the home-built TDFA with different pump power. We use the backward ASE of the 25 cm Tm^{3+} -doped silica fiber as probe signal. The fiber is pumped by ECL laser diode combined with a high power EDFA (PriTel, FA-33). We can get its optical spectrum by the OSA. Then amplify this backward ASE with the home-built TDFA. The home-built TDFA is pumped by a second high power EDFA. We can get the different amplified backward ASE by changing the pump power. The gain of this TDFA can be obtained by comparing amplified backward ASE with original backward ASE.

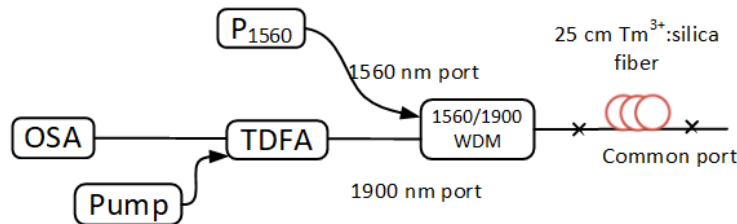


Figure 3.9: Experimental setup to measure the gain of the home-built TDFA

The optical spectra of the original backward ASE and amplified ASE are shown in Fig. 3.10. The original backward ASE is drawn by bold blue line. The different shape of spectra between original backward ASE and amplified ASE is caused by WDM coupler's insertion loss. From the results we can see that the insertion loss of this TDFA is around 20.57dB at 1874 nm, and when the pump power is 218 mW, the TDFA is transparent for 1874 nm signal. There are some lasing peaks shown around $1.9 \mu\text{m}$ when the pump power is larger than 1 W. That is due to the reflection at interfaces such as fiber connectors provide a feedback to thulium doped fiber in TDFA, which technically forms a laser cavity. When the gain of this laser cavity is larger than its loss, laser peaks show up.

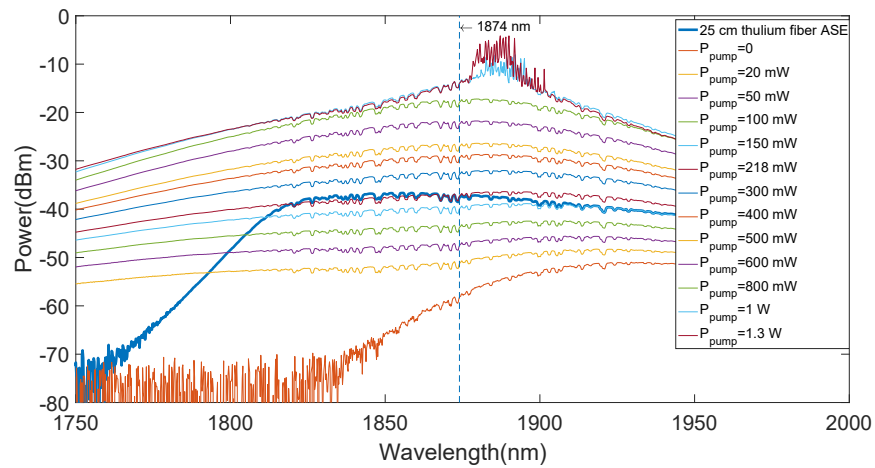


Figure 3.10: Optical spectra of the original backward ASE and amplified ASE

By analyzing spectra, we can get a plot showing gain at 1874 nm with respect to the pump power, demonstrated in Fig. 3.11. Since the input signal is the backward ASE, its power is lower than -20 dBm. This input power do not lead to saturation of the amplifier. The amplifier is operated under a small signal gain regime. It shows a gain saturation when the pump power is larger than 1 W with a maximum gain of 24.7 dB. The maximum gain coefficient of the TDFA is 0.145 dB/mW.

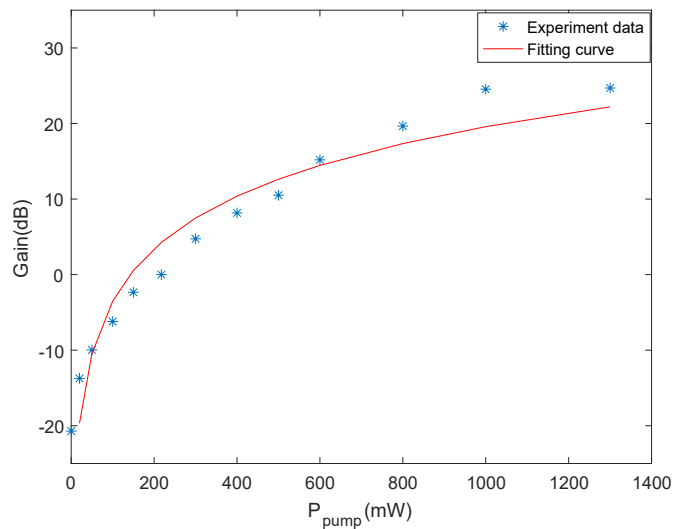


Figure 3.11: Gain at 1874 nm versus pump power for the Tm^{3+} doped fiber

3.3.3 Linear Cavity of the Brillouin TDFL

Fig. 3.12 shows a schematic of the multi-wavelength Brillouin TDFL in a linear cavity. The Brillouin gain medium is a 1 km long highly nonlinear fiber (OFS, HNLF Standard) with dispersion coefficient of $9.09 \text{ ps}/(\text{nm}\cdot\text{km})$ and dispersion slope of $0.02 \text{ ps}/(\text{nm}^2\cdot\text{km})$ at $1.9 \mu\text{m}$. The HNLF has an attenuation of $3.47 \text{ dB}/\text{km}$ and an effective area of $11.6 \mu\text{m}^2$. The Brillouin pump source consists of the home-built Brillouin pump laser, a home-built TDFA and an isolator. The isolator is employed in the BP to avoid the interference between the reflected light and Brillouin pump signal. The BP has a maximum power of approximately 100 mW at 1874 nm . The BP signal is coupled into the linear cavity by a 50:50 optical coupler. A loop mirror and a gold-tipped mirror with reflectivity above 90 % serve as reflectors and define the linear cavity. An optical circulator together with the coupler connected to the BP act as a loop mirror. A second TDFA is used in the linear cavity to amplify both BP signal and Brillouin signals. An optical coupler with a splitting ratio of 87:13 is used to extract 13% of main cavity power as output power. The optical spectra is measured by an OSA (YOKOGAWA, AQ6375) with a resolution of 0.05 nm , and a 10 dB attenuator is used before the OSA to avoid damage.

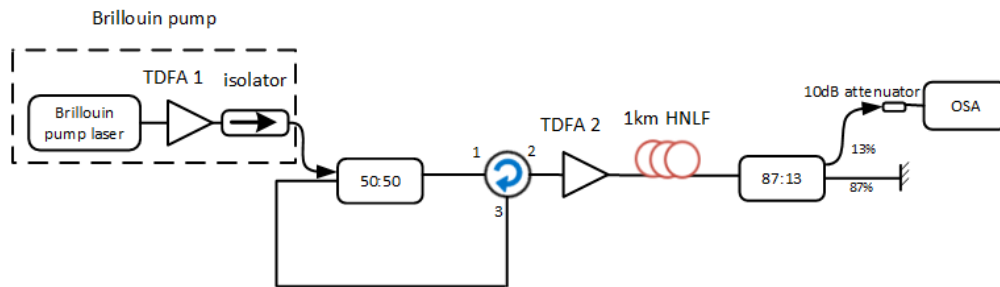


Figure 3.12: Multi-wavelength Brillouin TDFL configuration

The BP is injected into the linear cavity via the 50:50 coupler, the circulator and amplified by TDFA2, and then coupled into the HNLF to generate the first order Brillouin Stokes signal, which propagates in the opposite direction of the BP signal. This first order Brillouin signal is reflected by the loop mirror and amplified by the TDFA2 and coupled into the HNLF. Then 13% of the first order Brillouin output from the cavity by the coupler with a split ratio of 87:13, and the other 87% propagates to the gold-tipped mirror and

gets reflected back to complete a round trip oscillation. As long as the power of this signal is larger than the value of Brillouin threshold power, the second order Brillouin signal can be generated and oscillates in the cavity. This process continues until the Brillouin gain is smaller than the cavity loss, and subsequently generate cascaded Brillouin Stokes signals. By this mechanism, a multi-wavelength Brillouin TDFL is realized.

The Brillouin shift ν_B can be estimated by

$$\nu_B = \frac{2n_p v_a}{\lambda} \quad (3.1)$$

where v_a is the acoustic velocity within the fiber $v_a = 5.96$ km/s, the wavelength of the pump source $\lambda = 1873.9$ nm, the effective mode index at the pump wavelength $n_p = 1.45$. The estimated frequency shift $\nu_B = 9.22$ GHz, which is around 0.1 nm at 1874 nm.

3.3.4 Results and Discussion

The output spectra of the Brillouin TDFL are related to both BP power and the pump power of TDFA2 (intra-cavity TDFA). The most peak result are shown in Fig. 3.13. More than 100 peaks including anti-Stokes peaks can be observed in the result. The anti-Stokes peaks are generated by the four wave mixing (FWM). The Stokes peaks and anti-Stokes peaks cannot be separated with each other clearly and the measured ASE between adjacent peaks is relatively high, which is attributed to the low OSA resolution. With a high resolution spectrometer, a much clearer result can be achieved [44]. For this result, the BP power=70 mW, and TDFA2 pump power=1.5 W. In Fig. 3.13, the wavelength spacing is 0.1 nm, which agrees to our previous calculation.

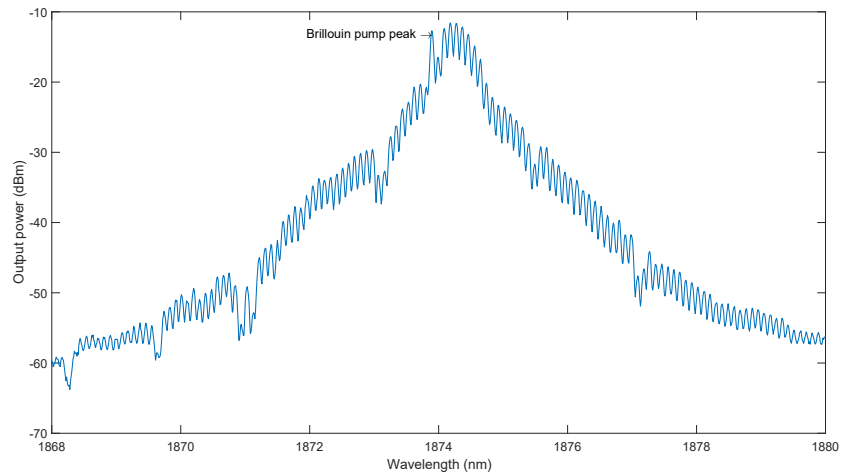


Figure 3.13: optical spectrum of the Brillouin TDFL when Brillouin pump power=70 mW, and TDFA2 pump power=1.5 W

Fig. 3.14 shows the spectra of the Brillouin TDFL with the TDFA2 pump increasing from 0.4 W to 1.2 W, where the BP power is fixed at 150 mW. The number of peaks increases with the TDFA2 pump power increases. This is due to the increment of TDFA gain that can easily compete with the Brillouin gain suppression.

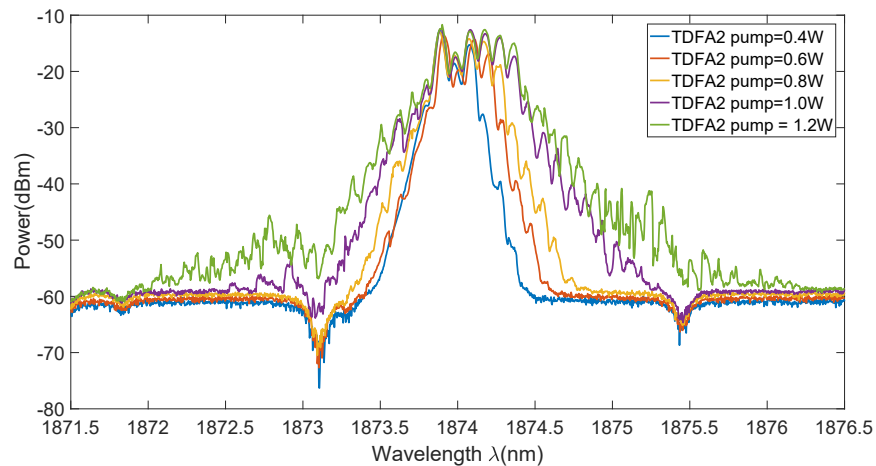


Figure 3.14: Spectra of the Brillouin TDFL with the BP power fixed at 150 mW

Fig. 3.15 shows the spectra of the Brillouin TDFL with the BP power increases from 30 mW to 70 mW with the pump power of TDFA2 fixed at 1.5 W. The BP power is measured after the isolator in Fig. 3.12. The peak number decreases with the BP power

increase because of the saturation effect in the Tm^{3+} -doped fiber of the TDFA, which led to insufficient signal power for the higher order to pump the HNLF, therefore stopping the process of multi-wavelength operation [45].

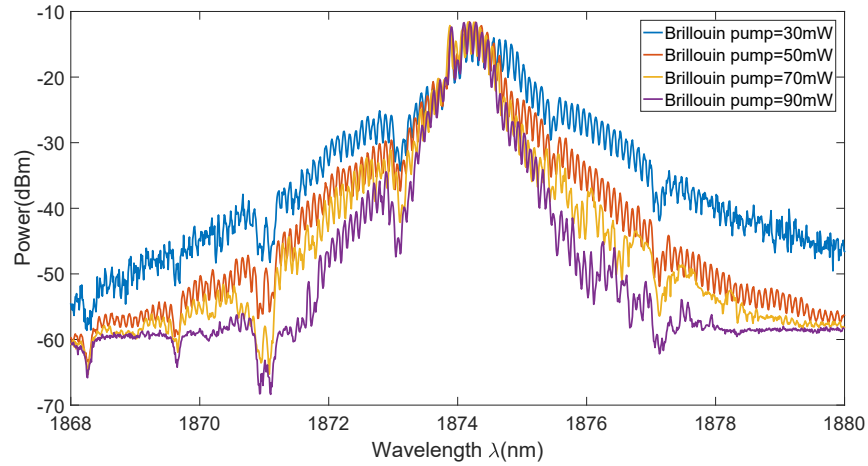


Figure 3.15: Spectra of the Brillouin TDFL with the TDFA2 pump power fixed at 1.5 W

During the experiments, we observe this interesting phenomenon, the first order Brillouin peak is always much weaker than the adjacent peaks, which is unexpected. To investigate the reason, we build the experimental setup in Fig. 3.16. It has the same linear cavity as the Brillouin TDFL but without Brillouin pump. It is a linear cavity laser. The gain medium of this laser is the Tm^{3+} -doped fiber in the TDFA2, and the pump source of this laser is the pump source of the TDFA2.

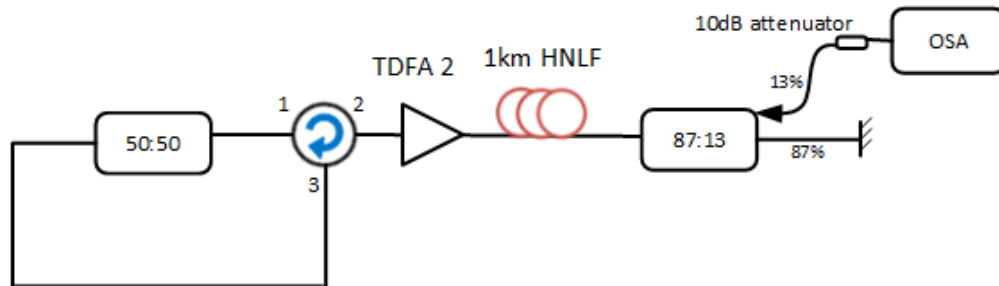


Figure 3.16: Experimental setup of the linear cavity laser

Fig. 3.17 compares the optical spectrum of the Brillouin TDFL with the linear cavity laser. From Fig. 3.17, we can see that both spectra of the linear cavity and Brillouin TDFL have some dips, and those dips overlap with each other in both spectra. One of the dips

is located at 1874 nm, which is the wavelength of the first order Brillouin peak. There are water vapour inside the OSA and those dips are generated by the water vapour absorption [46]. The first order Brillouin signal is absorbed by vapour in the OSA, that's why the first order Brillouin peak is much weaker than its adjacent peaks.

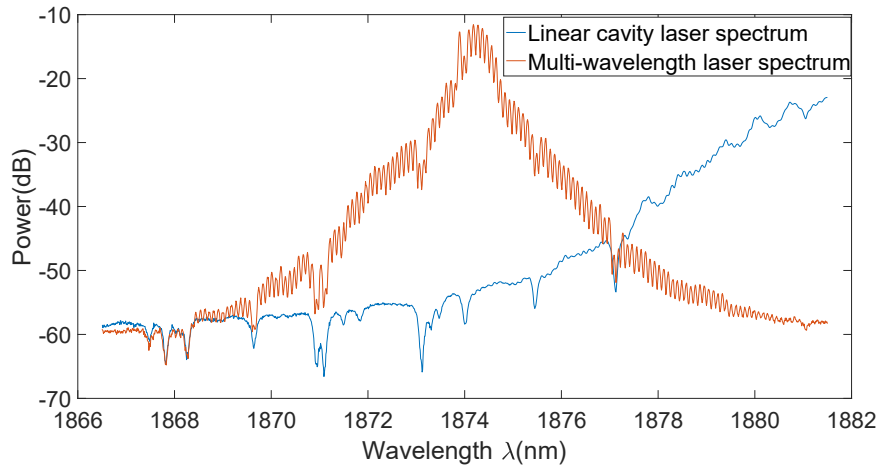


Figure 3.17: The optical spectra of the Brillouin TDFL and the linear cavity laser when the pump power is 1.5 W

The stability of this Brillouin TDFL is also investigated in 20 minutes. The optical spectra are shown in Fig. 3.18, and the peak wavelength and peak power fluctuations are shown in Fig. 3.19. Since the first order Brillouin peak is weaker due to the water absorption, and it is more sensitive to some other elements such as temperature, humidity and so on, we investigate the second order to fifth order Brillouin peaks. The wavelength drift of these four peaks are less than 0.02 nm and the power fluctuation are less than 3.4 dB in 20 minutes.

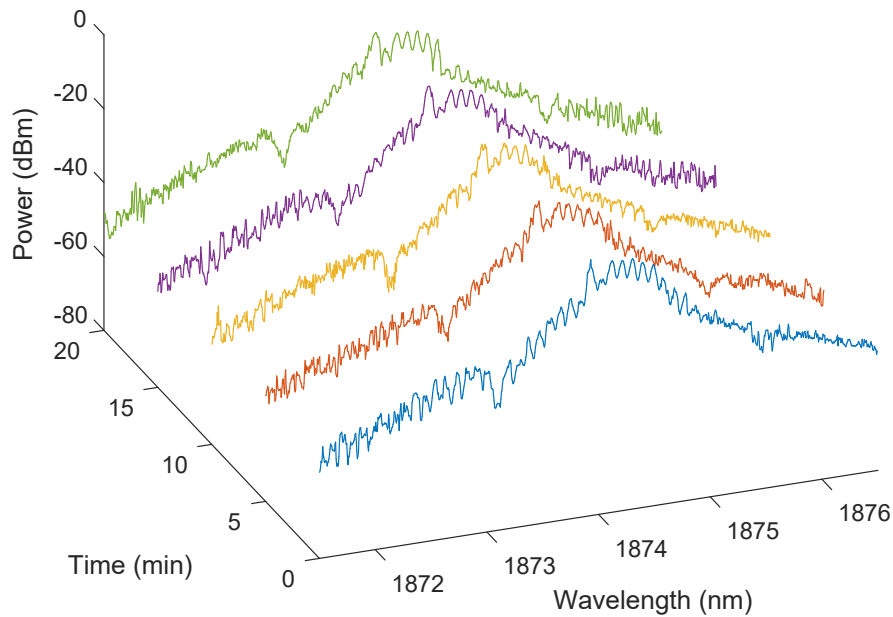


Figure 3.18: Output spectra of Brillouin TDFL measured in 20 minutes

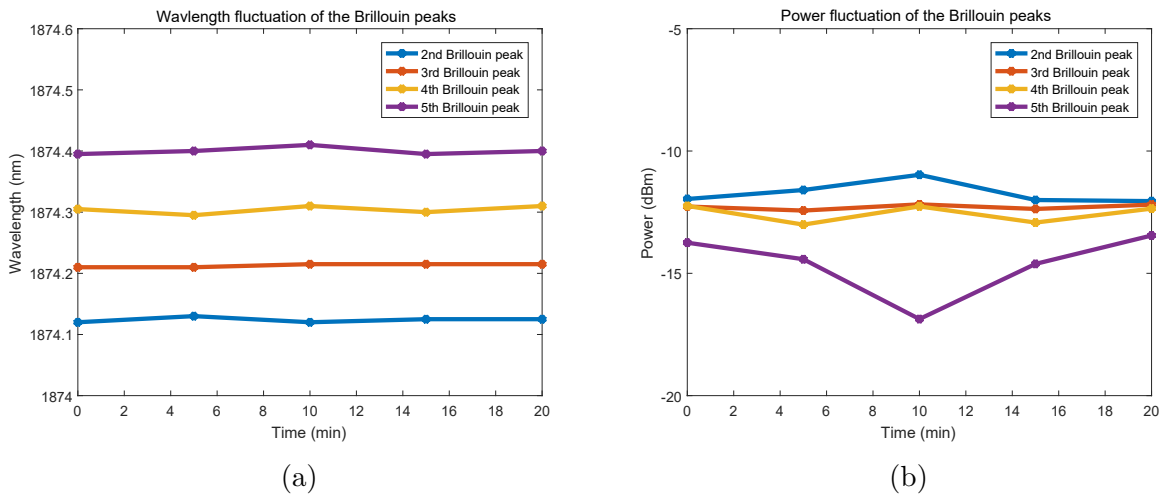


Figure 3.19: (a) wavelength fluctuations and (b) power fluctuations of four selected lasing peaks

As chapter 2 discussed, it is also possible to build a multi-wavelength Brillouin fiber laser with a ring cavity. However, the ring cavity configuration is not as simple as linear cavity. Besides, our experiments of ring cavity did not show as good results as the linear cavity

configuration.

3.4 Conclusion

In this chapter, we demonstrated the use of Tm^{3+} :silica DC fiber to realize a multi-wavelength TDFL with a linear cavity. With optimal pump operation, more than 100 Stokes and anti-Stokes lines can be observed in the optical spectrum. To the best of our knowledge, it is the most number of lasing wavelengths for a TDFL at around $2\ \mu\text{m}$. We also showed the stability of the laser. A 20 minutes test shows the peak powers fluctuate less than 3.4 dB and peak wavelengths drift less than 0.02 nm.

Chapter 4

CW Bismuth-Doped Fiber Lasers at 1726 nm

4.1 Introduction

In this chapter, we demonstrate BDFs in both linear cavity and ring cavity. The bismuth doped fiber is introduced first. Then we present BDFs with linear cavity and their outputs. The ring cavity setup is demonstrated at the end of the chapter.

4.2 Bismuth Doped Fiber

A 15 m long bismuth doped germanosilicate fiber fabricated by MCVD technique is used as active fiber in our experiments. The fiber was manufactured by Fiber Optic Research Center of the Russian Academy of Sciences. The fiber with 50 mol.% of germanium dioxide has a bismuth concentration of $10^5 \mu\text{m}^{-3}$, a core diameter of $125 \mu\text{m}$ and a cladding diameter of $125 \mu\text{m}$. The index difference between the core (1.52) and the cladding (1.45) of 0.07 results in a cutoff wavelength of $1.2 \mu\text{m}$. Fig. 4.1 shows the emission and absorption cross section spectra of the bismuth doped fiber, which is given by experimental data with theoretical extrapolation. The absorption spectrum peaks at 1650 nm, and the emission spectrum peaks at 1700 nm.

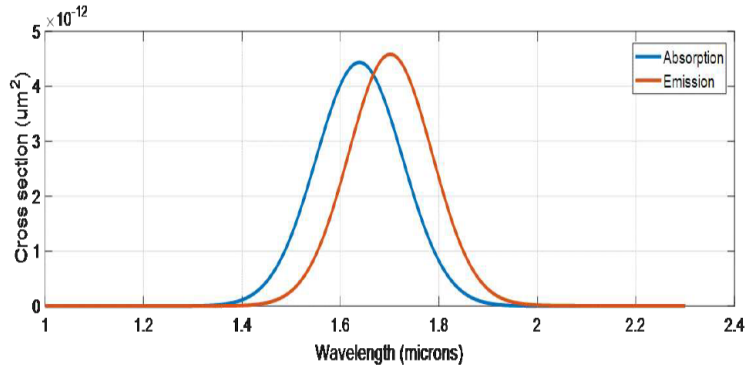
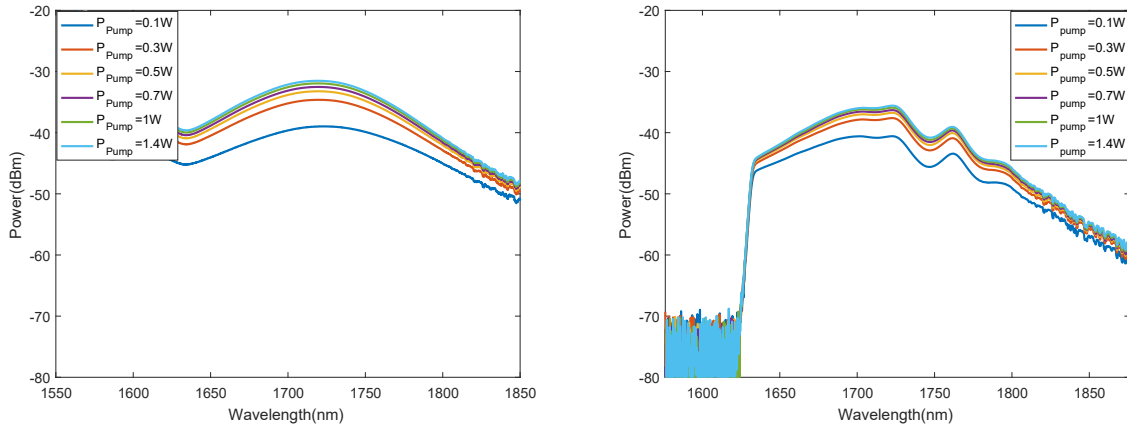


Figure 4.1: Spectra variation of the emission and absorption cross section

We also measure the forward and backward spectra of the fiber. The setups are similar to Fig. 3.1. The results are shown in Fig. 4.2. Compared with our Tm-doped fiber, bismuth fiber has lower ASE, which was caused by the bismuth ion property and the low bismuth ion concentration. From the results, we can see there is no big difference between forward ASE and backward ASE. Both forward and backward ASE have a peak value of approximately -35 dBm, and there is no obvious wavelength shift with pump power increase for both ASE spectra. Therefore, in the following experiments, we try both two pumping schemes.



(a) Forward ASE of the bismuth doped fiber (b) Backward ASE of the bismuth doped fiber

Figure 4.2: Optical spectra of the ASE for the bismuth doped fiber

To find the gain of the bismuth doped fiber, we design the following experiments. The experimental setups are shown in Fig. 4.3. In the forward pumping configuration, a supercontinuum is used as probe signal. The pump source is composed of a ECL laser diode at 1560 nm and a high power EDFA (PriTel, FA-33). The pump power can reach to 1.2

W. A optical coupler with splitting ratio of 90:10 is used to combine 10% probe signal and 90% pump signal into the bismuth doped fiber. An OSA is connected to the 1700 port of a 1550/1700 nm WDM coupler. The pump power is measured before the coupler by a power meter (Thorlabs, PM100D) along with a thermal power sensor (Thorlabs, S302C). The residual 1560 nm pump signal is eliminated by the WDM coupler to protect OSA. In the backward pumping configuration, there is a isolator to protect supercontinuum source.

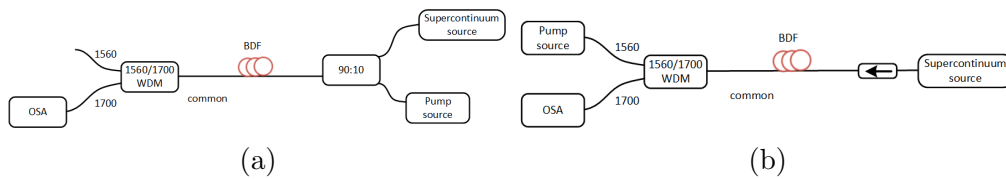


Figure 4.3: Experimental configurations to measure the gain of bismuth doped fiber with (a) forward pumping scheme and (b) backward pumping scheme

The optical spectra of the forward pumping scheme are demonstrated in Fig. 4.4. The original supercontinuum source spectrum is drawn by bold blue line. The sharp discontinuity around 1600 nm in optical spectra is caused by the 1560/1700 WDM coupler. It has a relatively large insertion loss from common port to 1700 nm port for wavelengths less than 1600 nm. When no pump power applied to the bismuth doped fiber, there is nothing except noise shown in the OSA, which means a strong absorption. As pump power increases, probe signal start to show in the OSA, and increases. From Fig. 4.4, we can see that when the pump power equals to 63 mW, the spectrum overlaps the supercontinuum spectrum at the 1726 nm, which means at this point, the gain equals to loss and the fiber is transparent to the 1726 nm signal. As pump power increases to the max, there is a gain region from 1600 nm to 1800 nm, and the maximum gain is around 10 dB at 1726 nm. The optical spectra of the backward pumping scheme are shown in Fig. 4.5. When the pump power is 114 mW, the gain equals to the loss at 1726 nm. The gain region is from 1660 nm to 1780 nm and the largest gain is around 6 dB when the pump power is maximum.

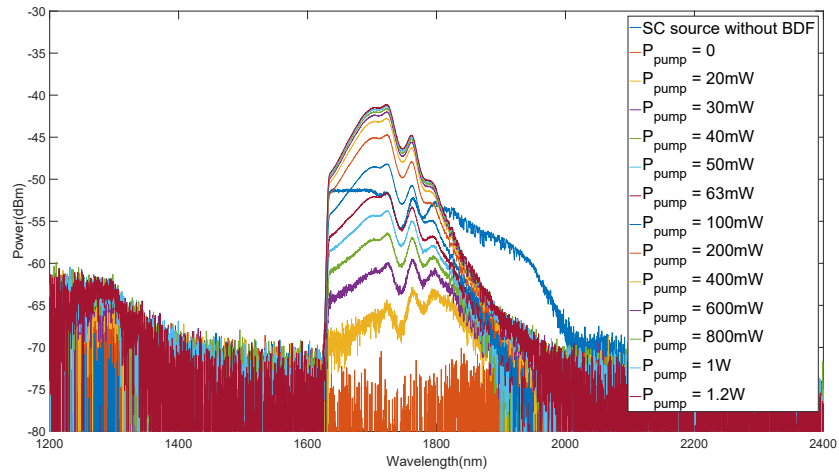


Figure 4.4: Optical spectra of the forward pumping scheme

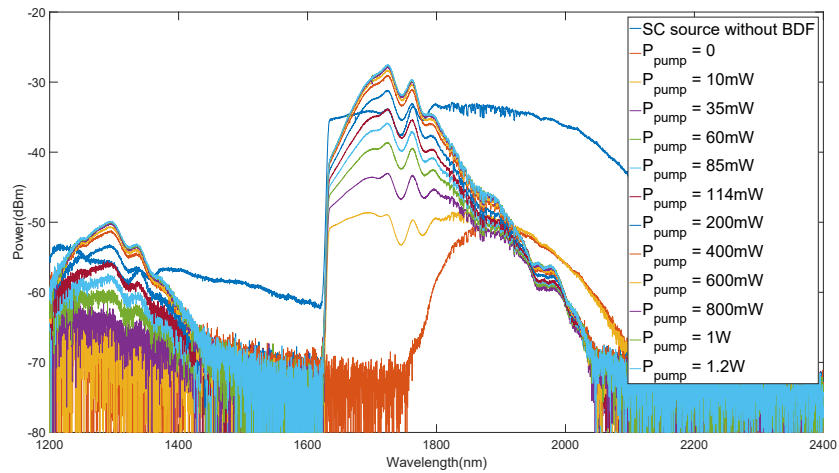


Figure 4.5: Optical spectra of the backward pumping scheme

By analyzing the optical spectra, we can get gain spectra of bismuth doped fiber with forward pumping (Fig. 4.6) and backward pumping (Fig. 4.7). When a spectrum is over 0 dB, the bismuth doped fiber amplifies the input signal. When a spectrum is less than 0 dB, the fiber absorbs the input signal.

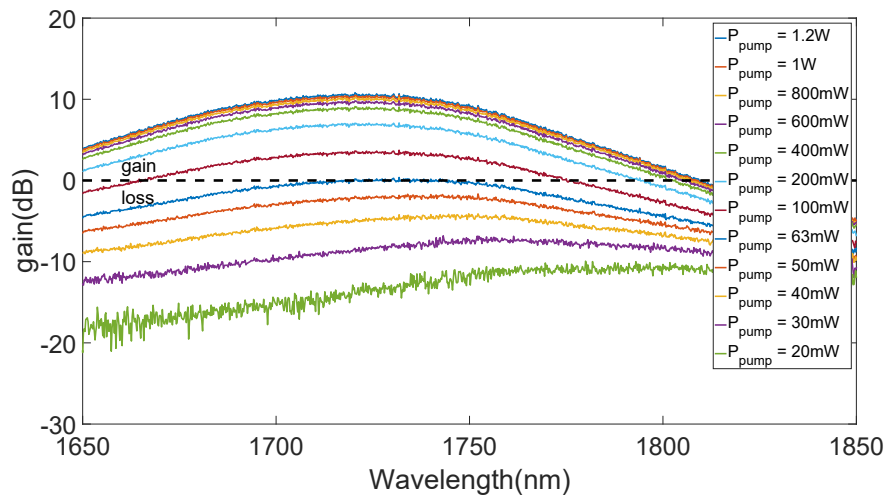


Figure 4.6: Gain spectra of bismuth doped fiber with forward pumping scheme

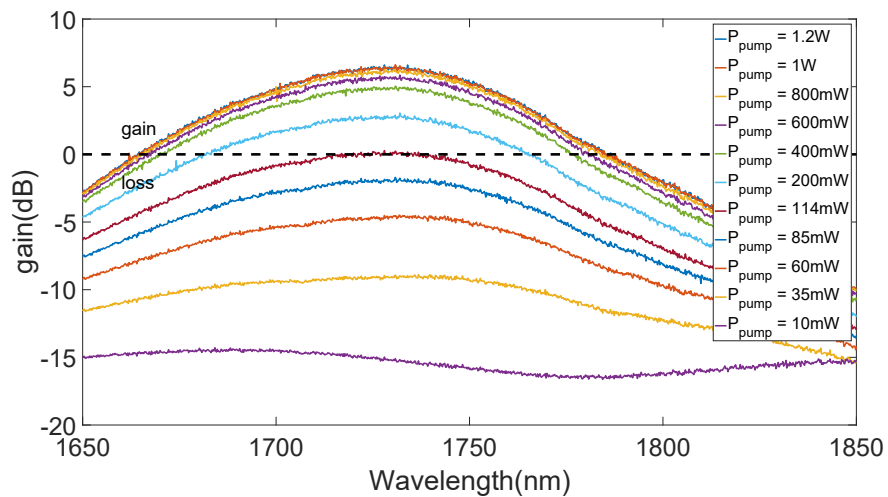


Figure 4.7: Gain spectra of bismuth doped fiber with backward pumping scheme

From the previous spectra, we can get a plot showing gain at 1726 nm with respect to the pump power, demonstrated in Fig. 4.8. There is a large absorption when pump power is 0. The value can not be measured precisely due to the low output of the supercontinuum source and the OSA sensitivity. For both forward pumping and backward pumping, when the pump power is smaller than 200 mW, the gains increase significantly. When the pump power is larger than 600 mW, there are gain saturations for both pumping schemes.

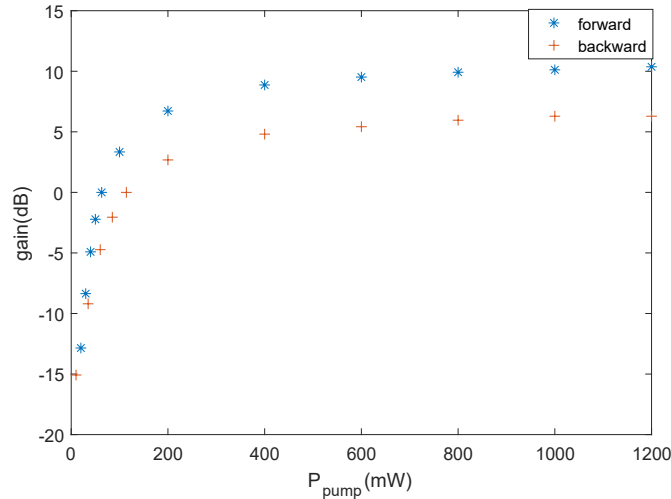


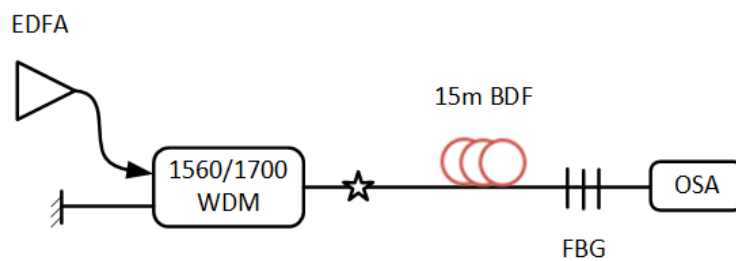
Figure 4.8: Gain at 1726 nm versus pump power for the bismuth doped fiber

4.3 Experimental Setups and Results

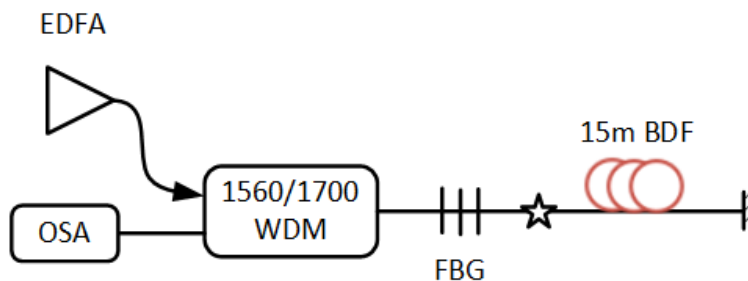
4.3.1 BDFL with Linear Cavity

Fig. 4.9 demonstrates the linear cavity BDFLs. The lasers are pumped by a high power EDFA (PriTel, FA-33), whose output power can be up to 1.4 W. The pump signal is launched into the laser cavity by a 1560/1700 nm WDM coupler. The pump power is measured at the star point. A FBG and a gold mirror are used as reflectors to compose the linear cavity. The FBG has a reflectivity of 95% at the center wavelength of 1726 nm with a 3 dB bandwidth of 0.4 nm. The insertion loss of the FBG is around 3 dB, which is mainly caused by splicing loss with SMF connectors. The gold mirror has a reflectivity of 90% at 1726 nm. Because the output contains pump signal, to get more accurate results, the output are measured by OSA (YOKOGAWA, AQ6375) instead of power meter.

The output spectra are shown in Fig. 4.10. When the pump power is low, there is a dip at 1726 nm, which is caused by the reflection of FBG. As pump power increases, the spectrum rises, and at some point, the lasers start lasing.

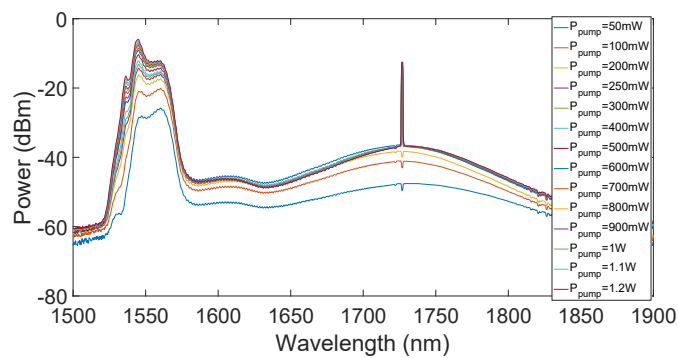


(a) Forward pumping scheme

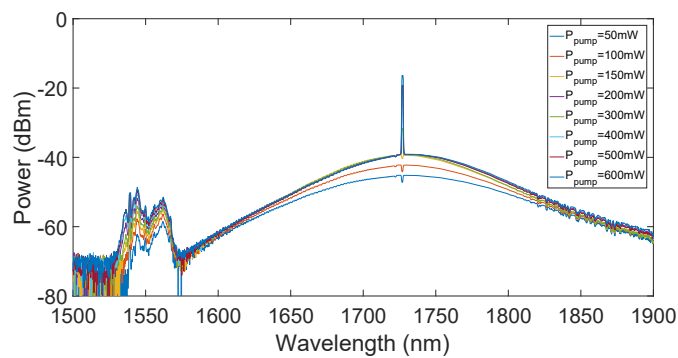


(b) Backward pumping scheme

Figure 4.9: Linear cavity BDFLs



(a) Forward pumping scheme



(b) Backward pumping scheme

Figure 4.10: Output spectra of linear cavity BDFLs

Fig. 4.11 shows the output power with respect to the pump power. Due to the insertion loss of the FBG, the maximum pump power launched into the cavity is lower for backward pumping scheme. Thus, backward pumping cavity has lower threshold power and output power. The slope efficiencies are 5.76×10^{-5} W/W and 4.99×10^{-5} W/W, respectively

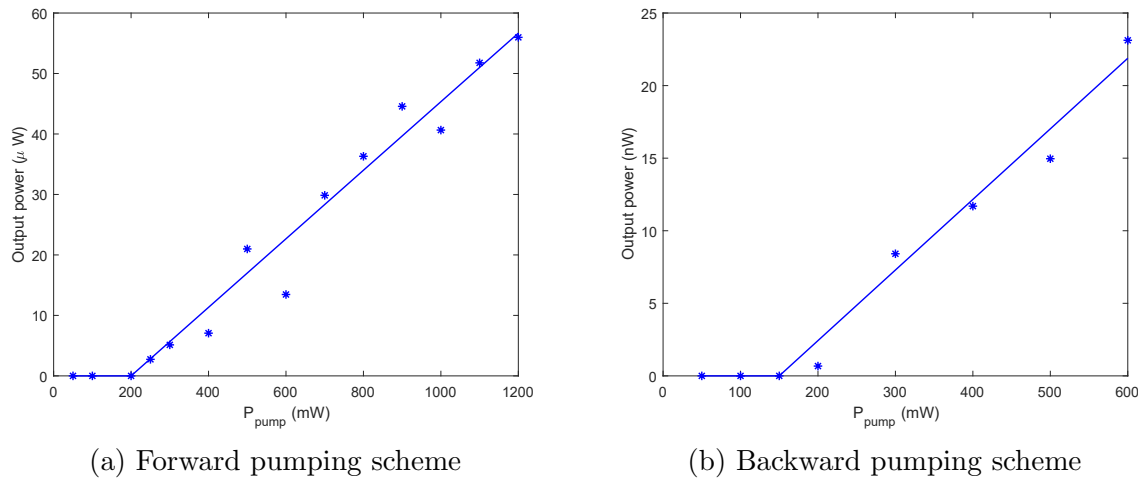


Figure 4.11: Output power with respect to the pump power for linear cavity BDFL

4.3.2 BDFL with Ring Cavity

Fig. 4.12 shows the ring cavity BDFL. A high power EDFA (PriTel, FA-33) serves as pump source, the pump signal is launched into the ring cavity by a 1550/1700 nm WDM coupler. The pump power is measured at the star point. The PC adjusts the polarization states. A isolator is used inside the cavity to make the lasing signal propagate counterclockwise. This design can also eliminates the residual pump signal inside the cavity. An optical coupler with splitting ratio of 90:10 extracts 10% to the output from the cavity. The total cavity length is around 25 m. Because there is no pump signal in the output, we use a power meter (EXFO, FPM-300) to measure the output power.

Fig. 4.13 demonstrates the output power with respect to the pump power. The threshold pump power is around 0.35 W and the slope efficiency is 3.55×10^{-4} W/W. When the pump power is increased up to 1.2 W, the laser has a output power of around 300 μW .

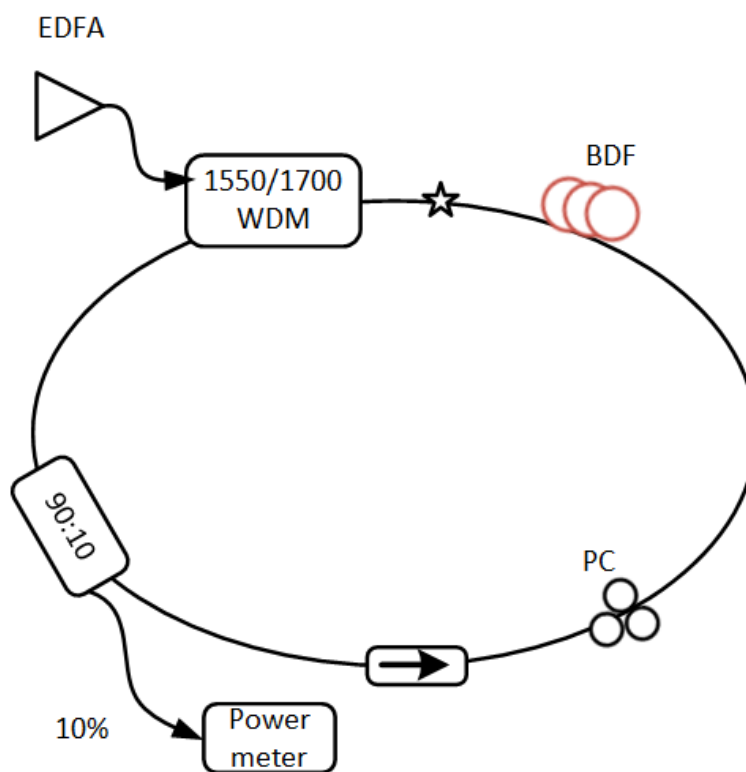


Figure 4.12: experimental setup of BDFL with ring cavity

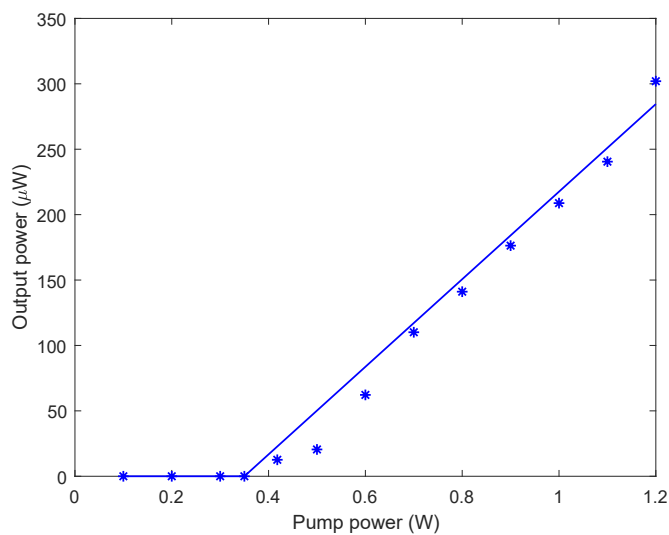


Figure 4.13: Output power with respect to the pump power for ring cavity BDFL

Fig. 4.14 shows the optical spectra of ring cavity BDFL. The laser is sensitive to polarization state. Adjusting the intra-cavity PC can control the number of peaks. Single-wavelength

at 1726 nm and dual-wavelength at 1726 and 1735 nm operation can show up. However, once the polarization state is fixed, the output of this laser is very stable, because the output stability mainly depends on birefringence, and the intra-cavity PC uses stress-induced birefringence to implement two independent wave plates to control the state of polarization of the transmitted light in SMF. Around 0.3 dB power fluctuation can be observed between different OSA scan.

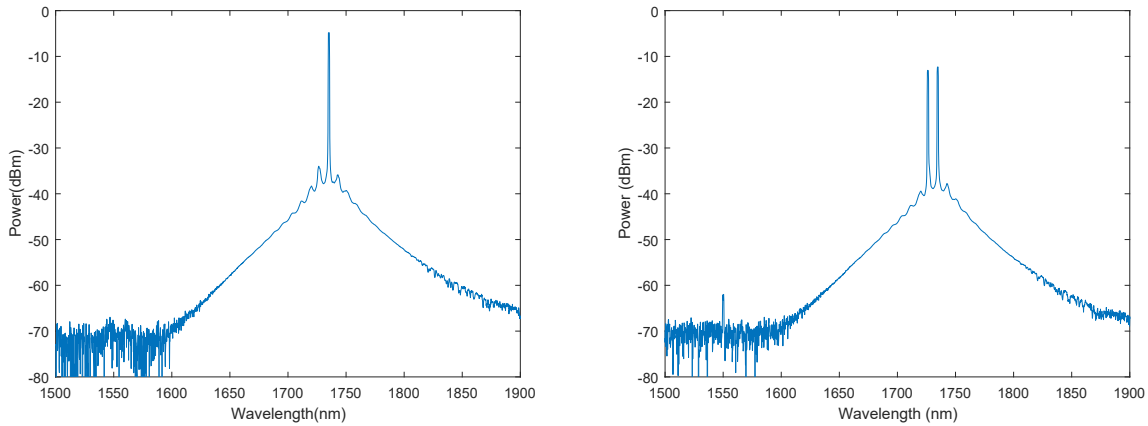


Figure 4.14: Optical spectra of ring cavity BDFL

4.4 Conclusion

In this chapter, we demonstrated the use of bismuth doped germanosilicate fiber to realize CW laser at 1.7 μm in both linear cavity and ring cavity. The linear cavity laser has maximum output power of 55 μm with slope efficiency of 5.76×10^{-5} W/W, while the ring cavity laser has maximum output power of 300 μm with slope efficiency of 3.55×10^{-4} W/W. By changing the polarization state, we are able to switch output operation between single-wavelength at 1726 nm and dual-wavelength at 1726 nm and 1735 nm. The investigation of BDFL could be useful for future researches.

Chapter 5

Conclusion

5.1 Summary

This thesis demonstrates two types of fiber lasers in near-infrared region. The first one is a multi-wavelength Brillouin TDFL in a linear cavity. More than 100 Stokes and anti-Stokes lines with wavelength spacing of 0.1 nm have been observed in the optical spectrum. This is, to the best of our knowledge, the most number of lines shown in optical spectrum for a Brillouin TDFL. A 20-minutes test shows that the peak power fluctuations and wavelength drifts are less than 3.4 dB and 0.02 nm, respectively. This Brillouin TDFL can provide a multi-wavelength laser source for telecommunication in 2 μm window as well as applications such as medicine, spectroscopy and sensing.

The second type of fiber lasers are CW BDFLs. Both linear cavity and ring cavity are used to build BDFLs in this work. Linear cavity BDFL has maximum output power of 55 μm with slope efficiency of 5.76×10^{-5} W/W. Ring cavity BDFL has maximum output power of 300 μm with slope efficiency of 3.55×10^{-4} W/W.

5.2 Future work

To further improve the performance of the Brillouin TDFL, a commercial narrow linewidth laser diode at 2 μm is required to serve as the seed of BP source. Compared with the home-

built TDFL, such a laser diode has a narrower linewidth, which will decrease the Brillouin threshold power and increase the number of Stokes and anti-Stokes lines. The output of the laser diode is more stable, which can improve the stabilization of the multi-wavelength Brillouin TDFL. Besides, using a laser diode can minimize the size of laser, make it more compact and simpler. Temperature control could be used to further stabilize the output peak powers and wavelengths.

Based on the current achievements in Brillouin TDFL. We propose the following future work on Brillouin TDFL. Due to linewidth narrowing effect of SBS, it is impossible to measure the linewidth of the Stokes and anti-Stokes signal by an OSA with resolution of 0.05 nm. To do such a work, we may need a high resolution spectrometer such as a optical complex spectrum analyzer or use a delayed self-heterodyne system [47] to measure the narrow linewidth.

To improve the performance of the BDFL, instead of using the 15 m bismuth doped fiber, a fiber with optimal length could be used in the laser to achieve the highest gain. To get a lower cavity loss, we can use some fiber devices with lower insertion losses and try some new splicing methods to lower the splicing loss.

Based on the current achievements in BDFL. We propose the following future work on BDFL. We can try to build a pulsed BDFL based on the NALM, nonlinear polarization rotation or saturable absorber such as graphene, CNT, etc. On the other hand, once we achieve a higher output power of the BDFL, we can try to build a multi-wavelength BDFL based on the SBS, FWM or nonlinear amplifier loop mirror.

References

- [1] T. H. Mainman. Stimulated optical radiation in ruby. *Nature*, 187:493–494, 1960.
- [2] A. E. Siegman. *Lasers*. University Science Books, 1986.
- [3] R. J. Mears, L. Reekie, I. M. Jauncey, and D. N. Payne. Low-noise erbium-doped fibre amplifier operating at $1.54\ \mu\text{m}$. *Electronics Letters*, 23:1026–1028, 1987.
- [4] F. Idachaba, D. U. Ike, and O. Hope. Future trends in fiber optics communication. In *Proceedings of the World Congress on Engineering*, volume I, 2014.
- [5] M. N. Petrovich, F. Poletti, J. P. Wooler, A. M. Heidt, N. K. Baddela, Z. Li, D. R. Gray, R. Slavík, F. Parmigiani, N. V. Wheeler, J. R. Hayes, E. Numkam, L. Grüner-Nielsen, B. Pálsdóttir, R. Phelan, B. Kelly, M. Becker, N. MacSuibhne, J. Zhao, F. C. Garcia Gunning, A. D. Ellis, P. Petropoulos, S. U. Alam, and D. J. Richardson. First demonstration of $2\ \mu\text{m}$ data transmission in a low-loss hollow core photonic bandgap fiber. In *Proceedings of the World Congress on Engineering*, 2012.
- [6] C. Jia, X. Liang, M. Rochette, and L. R. Chen. Alternate wavelength switching in a widely tunable dual-wavelength tm^{3+} -doped fiber laser at 1900 nm. *IEEE Photonics Journal*, 7(4), 2015.
- [7] K. Yin, B. Zhang, G. Xue, L. Li, and J. Hou. High-power all-fiber wavelength-tunable thulium doped fiber laser at $2\ \mu\text{m}$. *Optics Express*, 22(17):19947–52, 2014.
- [8] M. A. Chernysheva, A. A. Krylov, P. G. Kryukov, N. R. Arutyunyan, A. S. Pozharov, E. D. Obraztsova, and E. M. Dianov. Thulium-doped mode-locked all-fiber laser based on nalm and carbon nanotube saturable absorber. *Optics Express*, 20(26):124–30, 2012.

-
- [9] W. Peng, F. Yan, Q. Li, S. Liu, T. Feng, and S. Tan. A 1.97 μm multiwavelength thulium-doped silica fiber laser based on a nonlinear amplifier loop mirror. *Laser Physics Letters*, 10(11):115102, 2013.
- [10] X. Wang, Y. Zhu, P. Zhou, X. Wang, H. Xiao, and L. Si. Tunable, multiwavelength tm-doped fiber laser based on polarization rotation and four-wave-mixing effect. *Optics Express*, 21(22):25977, 2013.
- [11] T. Huang, X. Li, P. Shum, Q. Wang, X. Shao, L. Wang, H. Li, Z. Wu, and X. Dong. All-fiber multiwavelength thulium-doped laser assisted by four-wave mixing in highly germania-doped fiber. *Optics Express*, 23(1):340, 2015.
- [12] S. Liu, F. Yan, B. Wu, S. Tan, W. Peng, T. Feng, X. Liang, and Q. Li. A multiwavelength thulium-doped silica fiber laser incorporating a highly nonlinear fiber. *Journal of Optics*, 16(5):915–918, 2014.
- [13] S. V. Firstov, S. Alyshev, K. Riumkin, A. Khagai, A. Kharakhordin, M. Melkumov, and E. M. Dianov. Laser-active fibers doped with bismuth for a wavelength region of 1.6-1.8 μm . *IEEE Journal of Selected Topics in Quantum Electronics*, PP(99):1–1, 2018.
- [14] S. V. Firstov, V. F. Khopin, I. A. Bufetov, E. G. Firstova, A. N. Guryanov, and E. M. Dianov. Combined excitation-emission spectroscopy of bismuth active centers in optical fibers. *Optics Express*, 19(20):19551, 2011.
- [15] S. V. Firstov, S. V. Alyshev, K. E. Riumkin, V. F. Khopin, A. N. Guryanov, M. A. Melkumov, and E. M. Dianov. A 23-db bismuth-doped optical fiber amplifier for a 1700-nm band. *Scientific Reports*, 6:28939, 2016.
- [16] S. V. Firstov, S. V. Alyshev, K. E. Riumkin, M. A. Melkumov, O. I. Medvedkov, and E. M. Dianov. Watt-level, continuous-wave bismuth-doped all-fiber laser operating at 1.7 μm . *Optics Letters*, 40(18):4360, 2015.
- [17] T. Noronen, S. Firstov, E. Dianov, and O. G. Okhotnikov. 1700 nm dispersion managed mode-locked bismuth fiber laser. *Scientific Reports*, 6:24876, 2016.

-
- [18] J. Wang, S. Liang, Q. Kang, Y. Jung, S. Alam, and D. J. Richardson. Broadband silica-based thulium doped fiber amplifier employing multi-wavelength pumping. *Opt. Express*, 24(20):23001–23008, Oct 2016.
- [19] B. D. Frison. *Single and Dual-wavelength Lasing in the 800-820 nm and 1460 1520 nm Bands in a Thulium ZBLAN Fibre Laser*. McGill theses. McGill University Libraries, 2013.
- [20] I. A. Bufetov, M. A. Melkumov, S. V. Firstov, K. E. Riumkin, A. V. Shubin, V. F. Khopin, A. N. Guryanov, and E. M. Dianov. Bi-doped optical fibers and fiber lasers. *IEEE Journal of Selected Topics in Quantum Electronics*, 20(5):111–125, Sept 2014.
- [21] V. V. Dvoyrin, V. M. Mashinsky, L. I. Bulatov, I. A. Bufetov, A. V. Shubin, M. A. Melkumov, E. F. Kustov, E. M. Dianov, A. A. Umnikov, V. F. Khopin, M. V. Yashkov, and A. N. Guryanov. Bismuth-doped-glass optical fibers—a new active medium for lasers and amplifiers. *Opt. Lett.*, 31(20):2966–2968, Oct 2006.
- [22] G. Agrawal. *Nonlinear fiber optics*. Elsevier academic press, 2013.
- [23] R. Y. Chiao, C. H. Townes, and B. P. Stoicheff. Stimulated brillouin scattering and coherent generation of intense hypersonic waves. *Phys. Rev. Lett.*, 12:592–595, May 1964.
- [24] R. W. Boyd. *Nonlinear optics*. Elsevier academic press, 2008.
- [25] R. Stolen. Phase-matched-stimulated four-photon mixing in silica-fiber waveguides. *IEEE Journal of Quantum Electronics*, 11(3):100–103, Mar 1975.
- [26] G. J. Cowle and D. Y. Stepanov. Hybrid brillouin/erbium fiber laser. *Optics Letters*, 21(16):1250–2, 1996.
- [27] G. J. Cowle and D. Y. Stepanov. Multiple wavelength generation with brillouin/erbium fiber lasers. *IEEE Photonics Technology Letters*, 8(11):1465–1467, 1996.

-
- [28] D. D. Park, J. H. Park, N. Park, J. H. Lee, and J. S. Chang. 53-line multi-wavelength generation of brillouin/erbium fiber laser with enhanced stokes feedback coupling. In *Optical Fiber Communication Conference*, pages 11–13 vol.3, 2000.
- [29] M. H. Al-Mansoori, M. K. Abdullah, B. M. Ali, and M. A. Mahdi. Hybrid brillouin/erbium fibre laser in a linear cavity for multi-wavelength communication systems. *Optics & Laser Technology*, 37(5):387–390, 2005.
- [30] X. Wang, P. Zhou, X. Wang, H. Xiao, and L. Si. Multiwavelength brillouin-thulium fiber laser. *IEEE Photonics Journal*, 6(1):1–7, Feb 2014.
- [31] Y. Luo, Y. Tang, J. Yang, Y. Wang, S. Wang, K. Tao, L. Zhan, and J. Xu. High signal-to-noise ratio, single-frequency 2 μm brillouin fiber laser. *Opt. Lett.*, 39(9):2626–2628, May 2014.
- [32] F. Mihélic, D. Bacquet, J. Zemmouri, and P. Szriftgiser. Ultrahigh resolution spectral analysis based on a brillouin fiber laser. *Opt. Lett.*, 35(3):432–434, Feb 2010.
- [33] S. Fu, W. Shi, H. Zhang, Q. Sheng, G. Shi, X. Bai, and J. Yao. Linewidth-narrowed, linear-polarized single-frequency thulium-doped fiber laser based on stimulated brillouin scattering effect. *IEEE Photonics Journal*, 9(4):1–7, Aug 2017.
- [34] Y. Fujimoto and M. Nakatsuka. Infrared luminescence from bismuth-doped silica glass. *Japanese Journal of Applied Physics*, 40(3B):L279, 2001.
- [35] E. M. Dianov, V. V. Dvoyrin, V. M. Mashinsky, A. A. Umnikov, M. V. Yashkov, and A. N. Gur'yanov. Cw bismuth fibre laser. *Quantum Electronics*, 35(12):1083, 2005.
- [36] E. M. Dianov, A. V. Shubin, M. A. Melkumov, O. I. Medvedkov, and I. A. Bufetov. High-power cw bismuth-fiber lasers. *J. Opt. Soc. Am. B*, 24(8):1749–1755, Aug 2007.
- [37] E. M. Dianov, A. A. Krylov, V. V. Dvoyrin, V. M. Mashinsky, P. G. Kryukov, O. G. Okhotnikov, and M. Guina. Mode-locked bi-doped fiber laser. *J. Opt. Soc. Am. B*, 24(8):1807–1808, Aug 2007.

-
- [38] S. Firstov, S. Alyshev, M. Melkumov, K. Riumkin, A. Shubin, and E. Dianov. Bismuth-doped optical fibers and fiber lasers for a spectral region of 1600-1800 nm. *Opt. Lett.*, 39(24):6927–6930, Dec 2014.
- [39] A. Khagai, M. Melkumov, K. Riumkin, V. Khopin, S. Firstov, and E. Dianov. Nalmbased bismuth-doped fiber laser at 1.7 μm . *Opt. Lett.*, 43(5):1127–1130, Mar 2018.
- [40] C. Jia, J. Qiao, N. Abdukerim, M. Rochette, and L. R. Chen. Multi-wavelength brillouin tm₃₊-doped fiber laser at 1873 nm using a linear cavity. In *2017 IEEE Photonics Conference (IPC)*, pages 281–282, Oct 2017.
- [41] C. Jia, X. Liang, M. Rochette, and L. R. Chen. Alternate wavelength switching in a widely tunable dual-wavelength tm³⁺-doped fiber laser at 1900 nm. *Photonics Journal IEEE*, 7(4):1–7, 2015.
- [42] J. Zhang, C. Yue, G. W. Schinn, W. R. L. Clements, and J. W. Y. Lit. Stable single-mode compound-ring erbium-doped fiber laser. *Journal of Lightwave Technology*, 14(1):104–109, 1996.
- [43] J. Liu, J. Yao, J. Yao, and T. H. Yeap. Single-longitudinal-mode multiwavelength fiber ring laser. *IEEE Photonics Technology Letters*, 16(4):1020–1022, 2004.
- [44] W. Gao, M. Liao, T. Chen, T. Suzuki, and Y. Ohishi. Tunable brillouin-erbium comb fiber laser in a linear cavity with a single-mode tellurite fiber. *IEEE Photonics Technology Letters*, 25(1):51–54, 2012.
- [45] M. H. Al-Mansoori, M. K. Abd-Rahman, F. R. Mahamd Adikan, and M. A. Mahdi. Widely tunable linear cavity multiwavelength brillouin-erbium fiber lasers. *Optics Express*, 13(9):3471–6, 2005.
- [46] T. Yamanouchi and M. Tanaka. Absorption properties of the near-infrared water vapor bands. *Journal of Quantitative Spectroscopy and Radiative Transfer*, 34(6):463–472, 1985.

- [47] L. Richter, H. Mandelberg, M. Kruger, and P. McGrath. Linewidth determination from self-heterodyne measurements with subcoherence delay times. *IEEE Journal of Quantum Electronics*, 22(11):2070–2074, Nov 1986.